Research Square

Preprints are preliminary reports that have not undergone peer review.
They should not be considered conclusive, used to inform clinical practice,
or referenced by the media as validated information.

# Tailoring Polyaniline with Ionic Liquids for Sensing and Supercapacitor Applications

**Afeefa Saliha**
University of Calicut
**Sivakrishna Prakash**
University of Calicut
**Lijin Rajan**
University of Calicut
**Yahya A Ismail**
aiyahya@uoc.ac.in

University of Calicut

**Research Article**

**Keywords:** Conducting polymer, Polyaniline (PANI), Ionic liquid, Reactive sensing, Supercapacitors, Sensors

**Posted Date:** July 23rd, 2026

**DOI:** https://doi.org/10.21203/rs.3.rs-10124985/v1

**License:** This work is licensed under a Creative Commons Attribution 4.0 International License.
Read Full License

**Additional Declarations:** No competing interests reported.

# Tailoring Polyaniline with Ionic Liquids for Sensing and Supercapacitor Applications

Afeefa Saliha A M, Sivakrishna Prakash, Lijin Rajan, Yahya A Ismail*

*Advanced Materials Research Center, Department of Chemistry, University of Calicut, Thenhipalam, Kerala - 673635, India.*

*Corresponding author, Email: aiyahya@uoc.ac.in; aiyahya123@gmail.com*

## Abstract

Conducting polymers (CPs) have been identified as promising multifunctional materials capable of combining energy storage and self-sensing of working environment, as both functionalities arise from the same reversible redox reactions. Here, polyanilines (PANI) synthesized in protic ionic liquid (PIL) and aprotic ionic liquid (AIL) were studied to understand the effect of ionic liquids on these dual functionalities, and the results were compared with those of chemically synthesized PANI using $H_2SO_4$. PANI-PIL exhibited the highest electrical conductivity (~$10^{-1}$ S $cm^{-1}$), lowest contact angle (30°), and maximum reversible redox charge (9.7 mC). The electrochemical sensing characteristics were explored using cyclic voltammetry (CV) and chronopotentiometry (CP) by correlating the charge and energy consumed during the redox processes as a function of electrolyte concentration and applied current. PANI-PIL exhibited superior sensitivity toward electrolyte concentration (0.124) and electrical current (−1.01/0.93 mJ $mA^{-1}$). To account for the sensing characteristics of the material, a theoretical model based on redox charge-transfer is proposed. Galvanostatic charge–discharge studies reported specific capacitances of 277, 249, and 174 F $g^{-1}$ for PANI, PANI-PIL, and PANI-AIL, respectively, while PANI-PIL showed an enhanced cycling stability of 73.35% capacitance retention after 3000 cycles. Electrochemical impedance spectroscopy revealed lower resistance and faster ion diffusion in PANI-PIL, indicating enhanced ionic conductivity and charge transport. The incorporation of protic ionic liquid improves the overall performance of polyaniline by enhancing its conductivity, wettability, electrochemical reversibility, ion transport, and cycling stability,

highlighting ionic-liquid-mediated PANI as a promising material for integrated energy storage and electrochemical sensing applications.

Keywords: Conducting polymer, Polyaniline (PANI), Ionic liquid, Reactive sensing, Supercapacitors, Sensors

## 1. Introduction

The increasing demand for next generation electrochemical devices has shifted focus toward materials that can not only store energy efficiently but also actively sense and respond to their working environment[1-3]. Conducting polymers (CPs) have emerged as promising candidates due to their unique ability to integrate supercapacitive energy storage characteristics and reactive sensing capabilities within a single material platform. The same reversible electrochemical redox reactions are responsible for their fast charge storage characteristics while allowing CPs to sense the surrounding environmental changes by converting chemical or physical stimuli into measurable electrical signals. Such multifunctional behaviour is particularly attractive for applications in wearable electronics, smart sensors, and adaptive energy devices[4-7].

The origin of this combined behaviour lies in the conjugated backbone of CPs, which undergoes reversible rearrangements of $\sigma/\pi$ electrons during oxidation and reduction. These processes are intrinsically coupled with the insertion and expulsion of counter ions and solvent molecules, leading to changes in charge carrier density, chain conformation, and free volume within the polymer matrix. As a result, key properties such as conductivity, volume, optical response, and ion transport can be modulated in a controlled and reversible manner[8-10]. In supercapacitor applications, these fast faradaic reactions contribute to high charge storage capacity[11], while in reactive sensing variations in charge consumption, potential, or reaction kinetics reflect changes in the surrounding environment [10, 12],. The distinction between these functionalities is governed primarily by the extension and dynamics of redox process, which control both the electrochemical activity and sensitivity of the material.

Polyaniline (PANI), in particular, has received considerable attention due to its environmental stability, low cost, ease of synthesis, and highly tunable electrical

properties. Its electrochemical performance is strongly dependent on doping and dedoping processes, where the incorporation and removal of ionic species regulate charge transport and polymer chain configuration[13, 14]. Chemical doping typically involves the incorporation of dopants during synthesis, commonly through protonation using acids such as HCl or $H_2SO_4$ or through post-treatment processes[15] in which the polymer is exposed to suitable dopant media. While various methods have been developed to enhance the doping efficiency of polyaniline, ranging from the integration of carbonaceous nanomaterials like graphene oxide[16] to the use of secondary conducting polymers like PEDOT: PSS the selection of an optimal dopant remains a critical challenge[17]. Among these, ionic liquids (ILs) have emerged as particularly promising candidates, often surpassing traditional additives in both reliability and environmental safety. The primary advantage of ILs lies in their negligible vapor pressure and exceptional chemical stability; unlike volatile mineral acids which can leach out and cause spontaneous dedoping, ILs remain sequestered within the polymer matrix. This ensures that the PANI stays in its conductive emeraldine salt state for longer durations. At the molecular level, the bulky ions of the IL act as molecular spacers and plasticizers, encouraging a more ordered alignment of the polymer chains. This structural refinement not only lowers the resistance to charge transport but also allows for a highly tunable electrochemical response[18].

In recent years, ionic liquids (ILs), including protic ionic liquids (PILs) and aprotic ionic liquids (AILs), have emerged as versatile dopants and reaction media for CPs. The wide range of cation anion combinations enables precise control over polymer growth, doping level, and ion polymer interactions, while their ability to act as soft templates can influence chain assembly and morphology. Imidazolium-based ILs are particularly attractive due to their inherent acidity and potential for π-π interactions with aromatic monomers, allowing them to participate directly in the polymerisation process without additional acids[19, 20]. These features can enhance ion mobility, improve electrochemical activity, and tailor the multifunctional [21] behaviour of the resulting polymer. [22].

In the present work, we investigate the role of PILs and AILs in tuning the structural, electrochemical, and reactive sensing properties of PANI by synthesising the polymer in IL based media and comparing it with conventionally prepared $H_2SO_4$ doped PANI. Detailed electrochemical characterization was carried out using cyclic voltammetry (CV), galvanostatic charge-discharge (GCD), chronopotentiometry, and coulovoltammetry (Charge/ Potential plot (QV)), with particular emphasis on charge consumption behaviour and redox-driven responses. This study aims to establish a clear understanding of how ionic liquid mediated doping influences the interplay between supercapacitive performance and reactive sensing capability in PANI. By elucidating the role of ion-polymer interactions in governing charge storage and environmental responsiveness, this work contributes to the development of advanced multifunctional electrode materials for integrated energy storage and sensing applications.

## 2. Materials

Aniline and sulfuric acid (Fisher Scientific,99% purity), Ammonium persulfate (Loba Chemie 98%), Toluene (Qualigens 99.0%), Dimethyl sulfate (HiMedia 99.0%), 1-Methylimidazole (Spectrochem 99.0%) and imidazole (HiMedia 99.0%). All chemicals were of analytical grade and used as received, except aniline, which was freshly distilled under reduced pressure and stored below 5°C before use. Deionized water was used throughout all synthesis and washing.

### *2.1 Synthesis of Polyaniline*

Polyaniline (PANI) was synthesized via chemical oxidative polymerization of aniline using ammonium persulfate as oxidant. 0.02 mol of distilled aniline was dissolved in 150 mL of 1 M $H_2SO_4$ kept at ≤10°C and stirred for 15 min. Subsequently, 0.025 mol of APS dissolved in 50 mL of 1 M $H_2SO_4$ was added dropwise with continuous stirring for 1 h. The polymerization reaction was allowed to proceed for 8 h to obtain PANI in its emeraldine salt form. The resulting products were filtered, washed with double distilled water and acetone, and dried at 60°C in a hot air oven.

### *2.2. Synthesis of PANI from ionic liquids*

For ionic liquid-mediated synthesis, 0.01 mol of aniline was dissolved in 40 mL of freshly prepared ionic liquid and stirred in an ice bath for 30 min. The protic ionic liquid (PIL) was synthesized by reacting imidazole with dimethyl sulfate, while the aprotic ionic liquid (AIL) was prepared from 1-methylimidazole and dimethyl sulfate. 0.0125 mol of ammonium persulfate (APS) was added dropwise to the reaction media under continuous stirring, and the polymerization was allowed to proceed at 0 °C for 24 h. The resulting polymers were collected by filtration, thoroughly washed with distilled water followed by acetone to remove residual reactants and oligomers, and dried overnight at 60 °C. The synthesized samples were designated as PANI-$H_2SO_4$, PANI-PIL, and PANI-AIL .

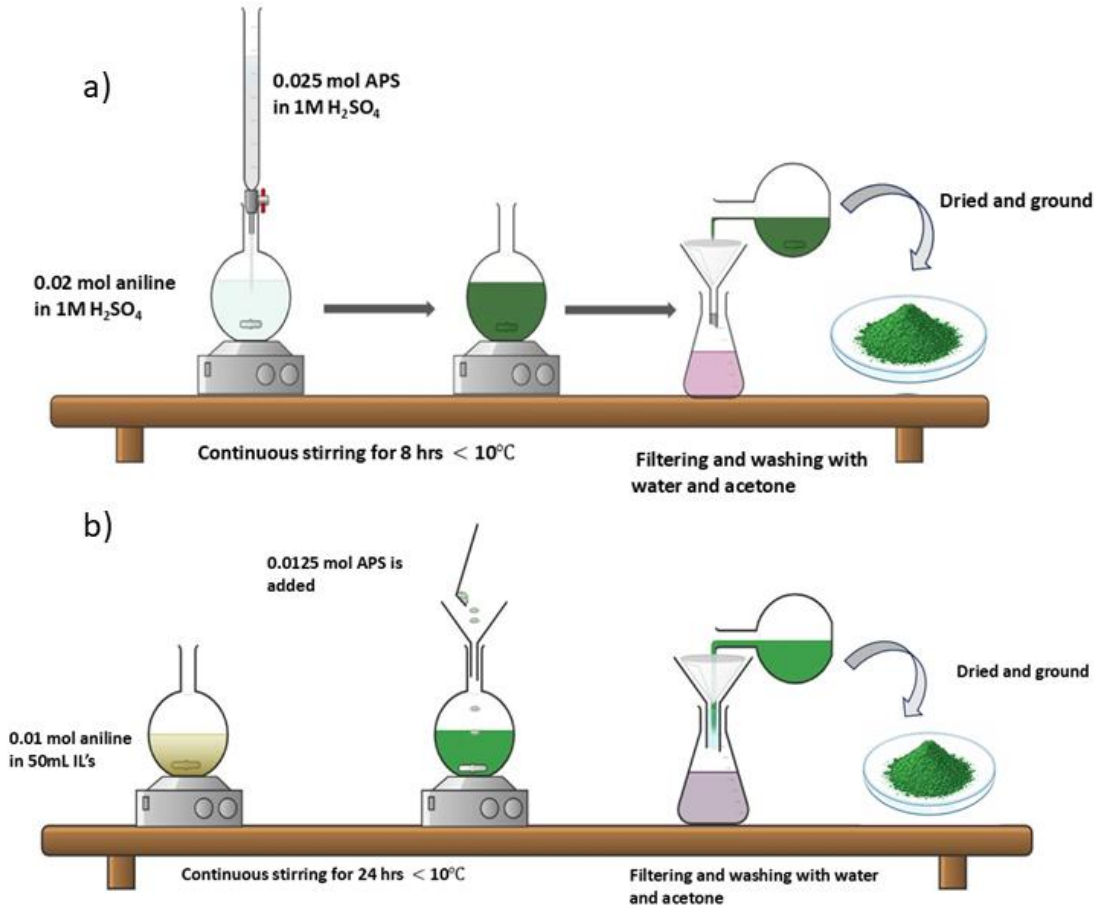



Figure 1: Schematic representation of a) synthesis of PANI. b) of synthesis of PANI in IL's

## 2.3 Characterization

Fourier transform infrared (FTIR) spectra were recorded using a JASCO FT/IR-4100 spectrophotometer (Japan). UV-visible spectra were carried out on a Jasco V-550 UV-Vis spectrophotometer (Portland, OR, USA). X-ray diffraction (XRD) analysis was performed using a Malvern P analytical X'Pert³ powder X-ray diffractometer (UK). Electrical conductivity measurements were carried out at room temperature and ambient pressure using a broadband dielectric spectrometer (BDS Novocontrol alpha analyser, Germany ) from with a two-probe configuration. All electrochemical studies were conducted using a Zahner Zennium Pro electrochemical workstation (Germany), controlled by Thales XT electrochemical software. The impedance data were analyzed using equivalent circuit modelling with ZSimpWin 3.21 to understand the charge transport and interfacial processes.

The electrochemical performance of PANI, PANI-PIL, and PANI-AIL was systematically evaluated using cyclic voltammetry (CV), coulovoltammetry (charge-potential, Q-V, analysis), chronopotentiometry (CP), galvanostatic charge–discharge (GCD), and electrochemical impedance spectroscopy (EIS) techniques.

# 3. Results and Discussion

## 3.1 General characterization

### *3.1.1* FTIR-ATR analysis

The FTIR spectra recorded in the range of 4000-500 $cm^{-1}$ are shown in Figure 2. The FTIR spectrum of pristine PANI exhibits characteristic peaks at 3438, 1570, 1472, 1309, and 1107 $cm^{-1}$, which correspond to N-H stretching vibration, C=C stretching of quinoid and benzenoid rings, and C-N stretching vibration of the benzenoid unit, respectively, confirming the formation of emeraldine salt form of PANI[23]. Similarly, the PANI-PIL shows bands at 3452, 1585, 1491, 1309, and 1121 $cm^{-1}$, which respectively representing N-H stretching, C=C stretching of quinoid and benzenoid rings, and C-N stretching vibration of the PANI backbone. In addition, PANI-PIL exhibited new absorption peaks at 1389, 1240, 818, and 593 $cm^{-1}$, which are attributed to the vibrational modes of the methyl imidazolium cation and C-O-$SO_3$ related

stretching and bending vibrations. These additional peaks confirm the successful incorporation of ionic liquid into the PANI matrix[24, 25]. The FTIR spectrum of PANI-AIL shows similar spectral features with peaks located at 3459, 1591, 1492, 1294, 1134, 1394, and 1041 $cm^{-1}$, corresponding to N-H stretching, C=C stretching of benzenoid and quinoid rings, C-N stretching vibration, imidazolium ring vibrations, and C-O-$SO_3$ stretching and bending modes respectively[26]. Notably, the peaks observed in PANI-PIL and PANI-AIL exhibit slight shifts toward higher wavenumbers compared to pristine PANI, indicating strong molecular interaction and enhanced protonation of PANI chains due to ionic liquid doping. This effect is more pronounced in PANI-PIL owing to the presence of a labile proton in the protic ionic liquid, which facilitates greater protonation along with stroger hydrogen bonding and electrostatic interactions.

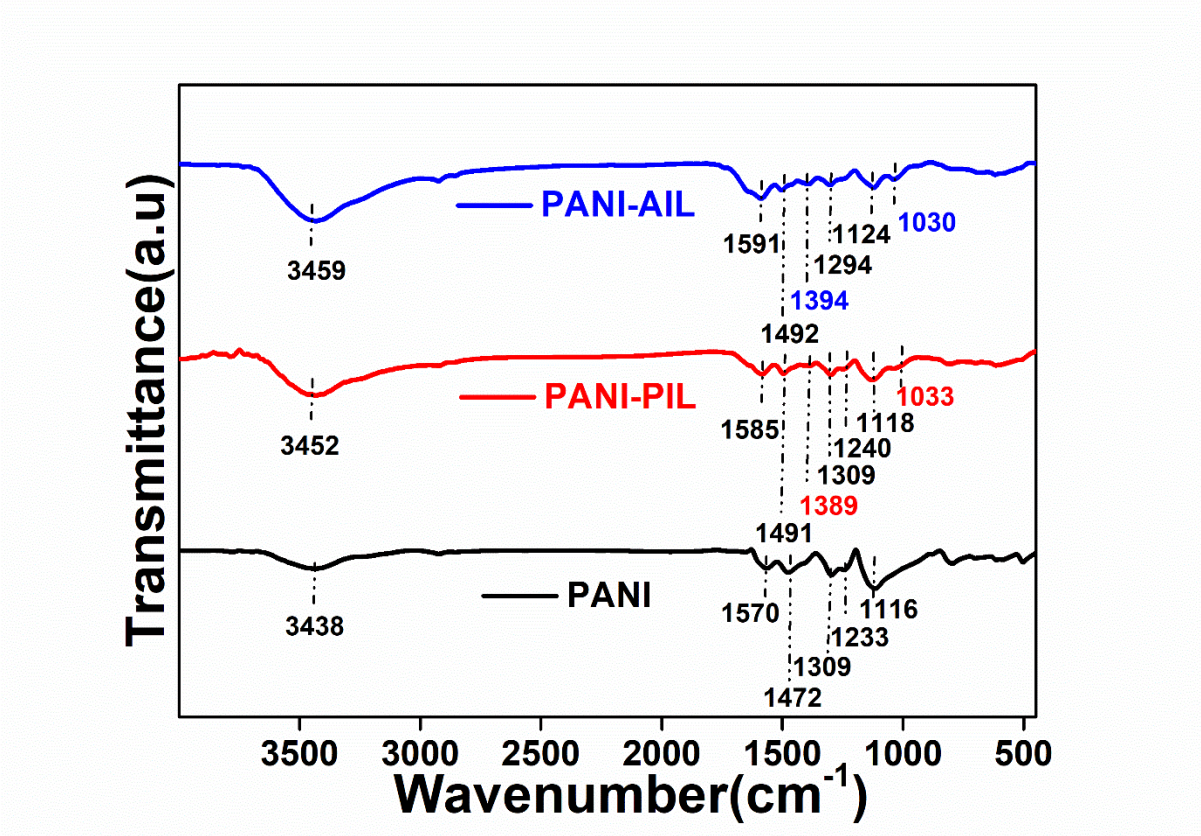



***Figure 2**: FTIR spectrum of PANI-AIL, PANI-PIL, PANI*

### *3.1.2 UV-Visible spectra*

The electronic structure of the polymers was explored using UV-Visible spectroscopy, and the results are shown in Figure 3. PANI exhibits peaks at 326 nm, 445 nm, and 635 nm in its UV-Visible spectrum, corresponding to $\pi \rightarrow \pi^*$, $\pi \rightarrow$ polaron, and polaron $\rightarrow \pi^*$ transitions[27, 28], respectively. Similarly, PANI-AIL also showed these three characteristic absorption peaks at 331 nm, 444 nm, and 620 nm, representing $\pi \rightarrow \pi^*$, $\pi \rightarrow$ polaron, and polaron $\rightarrow \pi^*$ transitions. In the case of PANI-PIL, the absorption peaks occur around 332 nm, 445 nm, and 627 nm. When the transitions are closely observed it is seen that the $\pi \rightarrow \pi^*$ transition of PANI-PIL and PANI-AIL exhibits a bathochromic shift compared to PANI, while the $\pi \rightarrow$ polaron peak remains similar to PANI. Additionally, the polaron $\rightarrow \pi^*$ peak of PANI-PIL and PANI-AIL shows a hypsochromic shift in comparison to PANI. In addition, the Tauc equation was used for determining the optical bandgap energy ($E_g$). The $E_g$ value was obtained by extrapolating the linear portion of the $(\alpha h\upsilon)^2$ versus $h\upsilon$ plot until $\alpha$ (absorption coefficient) approaches zero and the plots are represented in figure 3 (b-d). PANI-PIL has the lowest $E_g$ among the samples, measuring 3.27 eV, while PANI and PANI-AIL have band gaps of 3.29 eV and 3.33 eV, respectively[29].

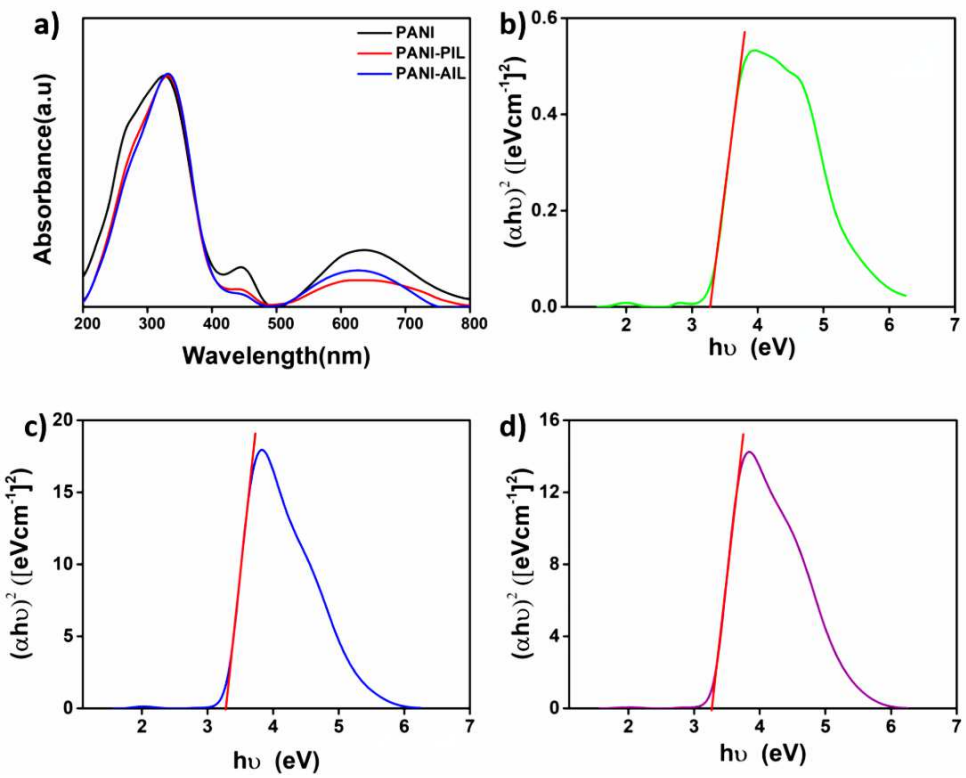



*Figure 3: UV-Visible spectra of a) PANI, PANI-AIL, and PANI-PIL, and Tauc plot of b) PANI, c) PANI-AIL, d) PANI-PIL.*

### *3.1.3 Thermogravimetric analysis*

Thermogravimetric analysis (TGA) was employed to analyze the thermal stability of PANI, PANI-PIL and PANI-AIL over the temperature range of 30°C to 600 °C. The TGA curves are shown in Figure 4, exhibit three distinct weight loss stages[30]. The initial weight loss observed around 100 °C is due to the evaporation of adsorbed moisture. A significant weight loss begins at approximately 240 °C, corresponding to the thermo-oxidative degradation of the PANI backbone along with the loss of dopant species. Among the samples, pristine PANI shows the most rapid degradation, indicating lower thermal stability. In comparison, PANI-AIL and PANI-PIL exhibit improved thermal resistance, with PANI-PIL retaining the highest residual weight at elevated temperatures. This enhanced thermal stability is likely due to stronger interactions between the PANI chains and the polymeric ionic liquid, which contribute to the structural integrity of the composite. The findings indicate that incorporation of

polymeric ionic liquids effectively enhances the thermal stability of PANI-based materials for advanced energy storage applications.

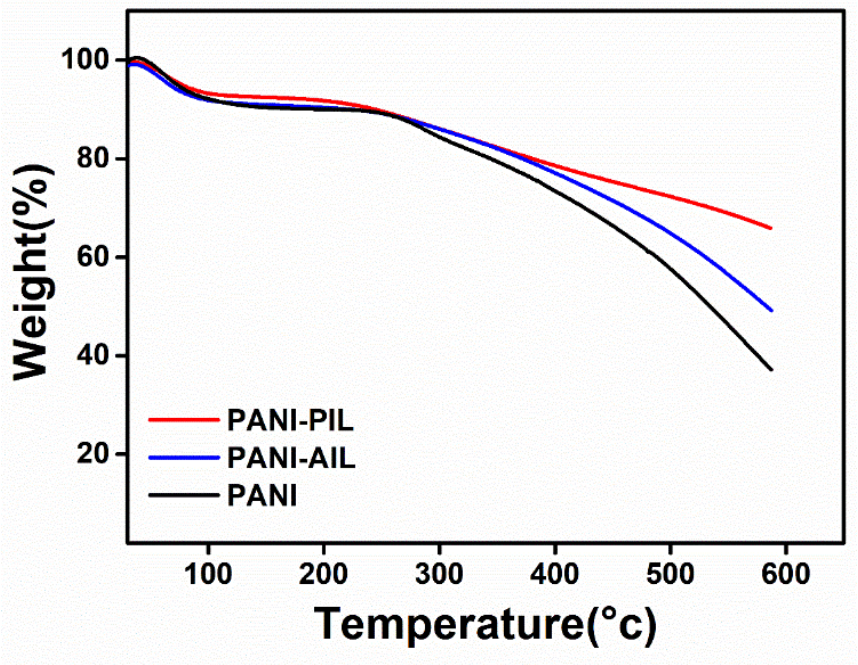



*Figure 4: TGA of PANI, PANI-AIL, and PANI-PIL.*

### *3.1.4 X-ray diffraction (XRD)*

The powder XRD spectra of all polymers are shown in Figure 5. The XRD spectra of pristine PANI revealed the presence of three distinct crystalline peaks around 10°, 15°, and 25°, accompanied by a broad amorphous diffraction peak at 20°. These XRD peaks at $2\theta \approx 10°$, 15°, 20°, and 25° correspond to the crystal planes 001, 011, 100, and 110, respectively, indicating that a significant proportion of PANI chains are aligned within these four crystal planes.

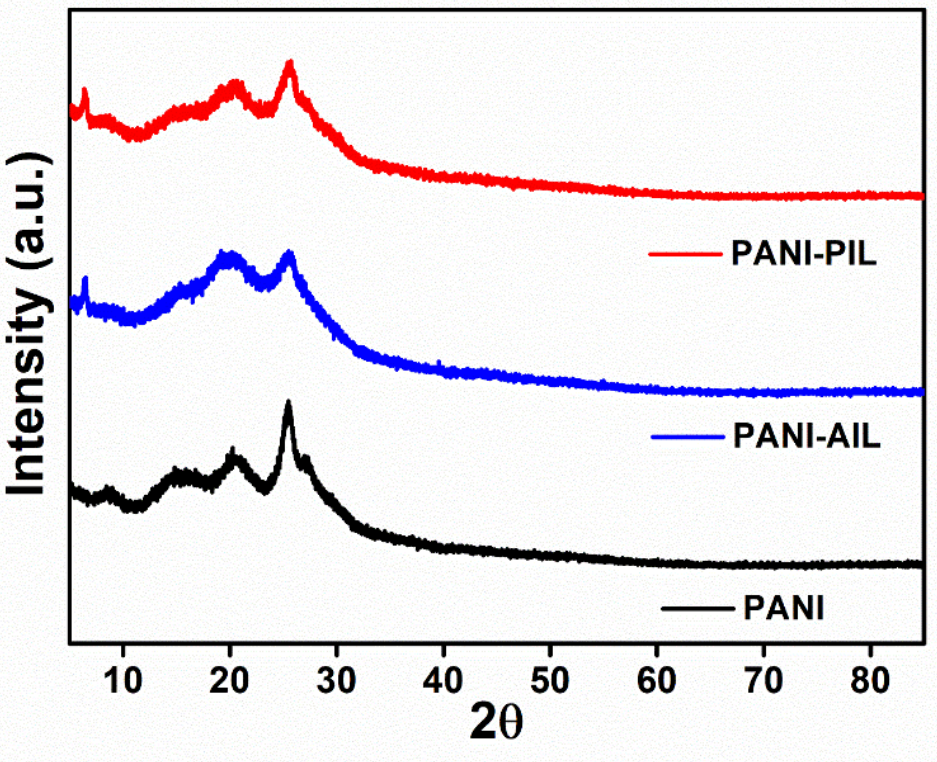



*Figure 5: XRD spectrum of PANI, PANI-AIL, and PANI-PIL*

### *3.1.5 Contact angle measurement*

Contact angle measurements were performed using water as the probe liquid. As shown in Figure 6, pristine PANI exhibited a contact angle of 49.7°. The contact angle increased slightly to 52.6° for PANI-AIL, indicating a decrease in surface hydrophilicity. In contrast, PANI-PIL exhibited a contact angle of 30°, indicating enhanced hydrophilicity, which may be attributed to the higher charge density and stronger polar interactions associated with the protic ionic liquid[31, 32]. The lower contact angle exhibited by PANI-PIL indicates enhanced interaction with the electrolyte, which may promote more efficient electrolyte diffusion compared to pristine PANI and PANI-AIL.

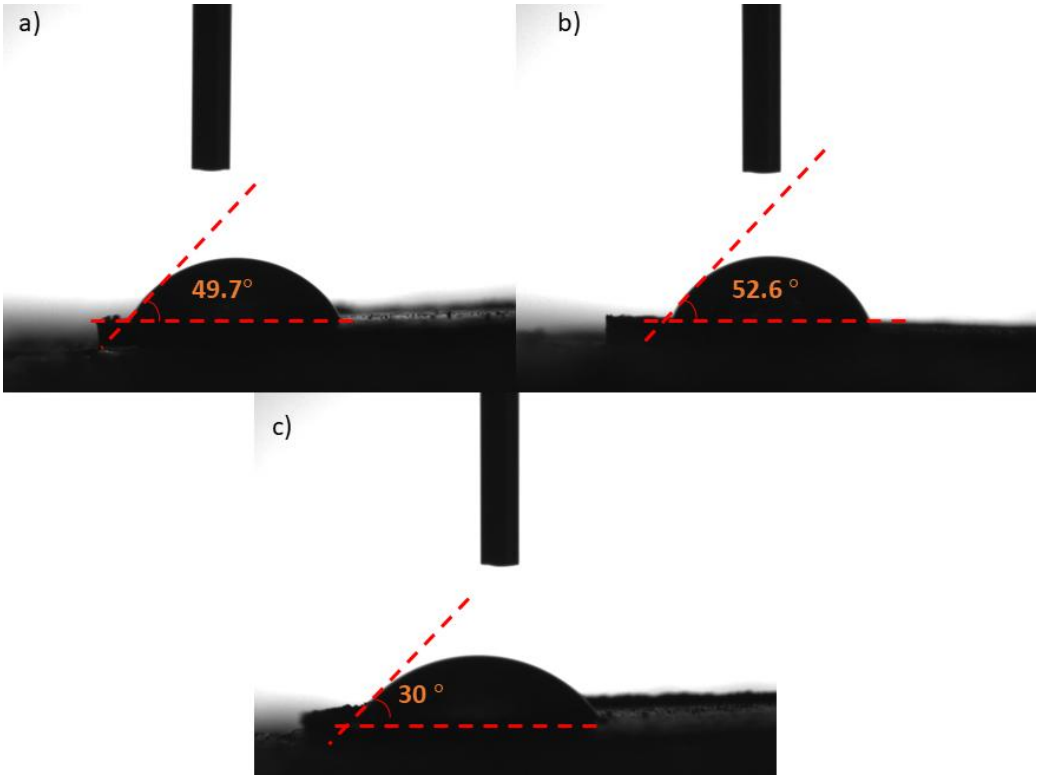



*Figure 6: Contact angle of a) PANI, b) PANI-AIL, and c) PANI-PIL*

### *3.1.6 FESEM analysis*

The morphology of the polymers was analysed using Scanning Electron Microscope (SEM) . The SEM images of PANI (Figure 7-c,f) revealed a uniform coral-like structure. The SEM analysis of PANI-AIL (Figure 7-b,e) displayed a significant change in morphology, transitioning from a coral-like structure to unevenly sized nano-particles. The irregular pattern observed in PANI-AIL may have reduced the effective surface area and hindered efficient ion transport during the charge discharge process. The structural variation could be responsible for the lower specific capacitance compared to PANI and PANI-PIL.On the other hand, the surface morphology of PANI-PIL (Figure 7-a,d) exhibited a coral-like structure similar to that of PANI with more uniform-sized particles which facilitated better electrochemical performance and charge storage behavior.[33]

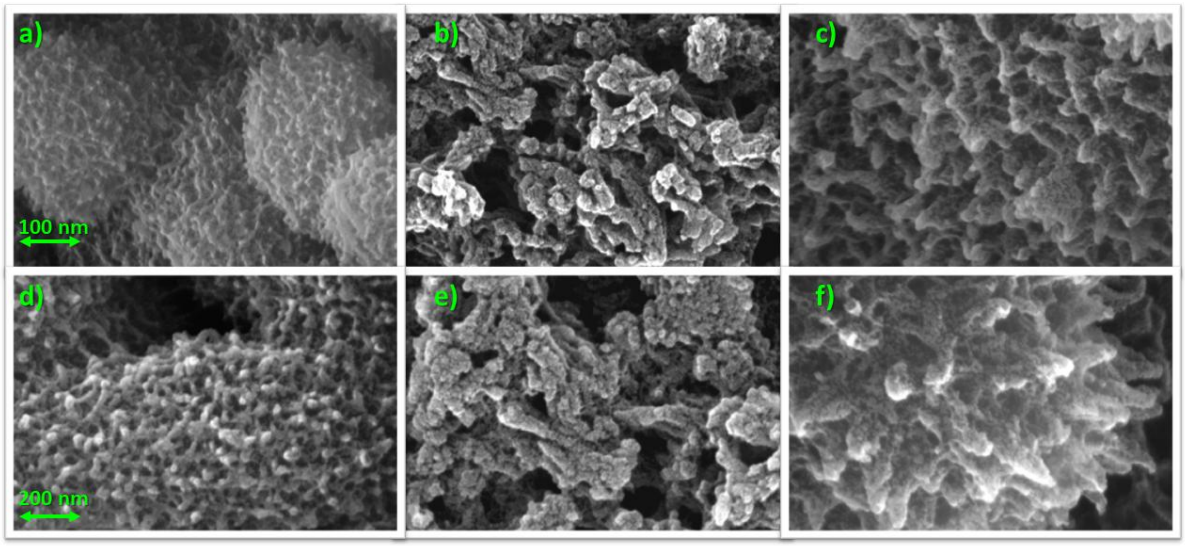



*Figure 7: SEM images of PANI-PIL, PANI-AIL and PANI at 100nm (a-c) and 200nm (d-f).*

### 3.1.7 Electrical conductivity studies

The frequency-dependent electrical conductivity of PANI, PANI-PIL, and PANI-AIL was measured over the frequency range of 1 Hz to $10^7$ Hz, as shown in Figure 8. All samples exhibited frequency-independent conductivity throughout the investigated frequency range, indicating dominant dc conduction and stable charge transport. Among the samples, PANI-PIL showed the highest conductivity (~$10^{-2}$ S $cm^{-1}$), which can be attributed to enhanced protonation, improved chain ordering, and facilitated charge transport in the presence of the protic ionic liquid. Pristine PANI exhibited intermediate conductivity, whereas PANI-AIL showed the lowest conductivity, likely due to reduced charge carrier mobility and increased structural disorder. [34].

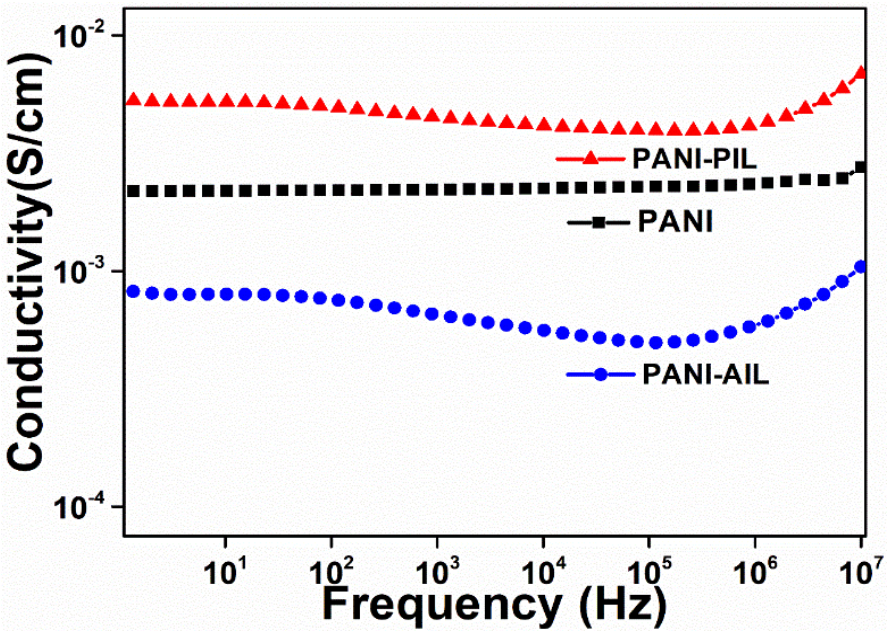



*Figure 8: Conductivity of PANI, PANI-AIL, and PANI-PIL*

### 3.2 Electrochemical characterisations

#### *3.2.1 Voltametric response*

The electrochemical behaviour of the synthesized polymers were investigated by cyclic voltammetry (CV). Figure 9a presents the CVs of PANI, PANI-PIL, PANI-AIL were recorded at the scan rate of 25 mV/s in 1M $H_2SO_4$ at room temperature. The Ag/AgCl used as the reference electrode platinum wire as counter electrode, and the polymer coated on a glassy carbon as the working electrode. Polyaniline (PANI) is known to exhibit multiple redox states, ranging from leucoemeraldine to pernigraniline, with intermediate stable states such as emeraldine, protoemeraldine, and nigraniline[16]. The CV plots exhibited characteristic redox couples within the potential ranges of 0.22-0.60 V and 0.48-0.44 V, corresponding to the leucoemeraldine/emeraldine and emeraldine/pernigraniline transitions, respectively[35, 36]. The CV of PANI-AIL closely resembles that of PANI synthesized in $H_2SO_4$, exhibiting two sets of redox couples at similar potentials, which suggests comparable redox mechanisms. Neverthless, the CV of PANI-PIL showed four distinct redox couples, suggesting the presence of more stabilized intermediate redox states. These redox couples are attributed to the sequential transitions of leucoemeraldine / emeraldine, emeraldine/ protoemeraldine, protoemeraldine/ nigraniline, and nigraniline / pernigraniline. The

higher current observed for PANI-PIL reflects improved capacitive behavior and enhanced electrochemical reversibility.

***Coulovoltammogram***

The number of electrons transported per polymer chain ($n_e^-$), which was calculated from the charge consumed during the reaction, was used to quantify the extension of the reversible redox process (reaction 1) [37, 38]. The voltammetric response provided a precise measurement of this charge. Coulovoltammogram (QV) was obtained by integrating the voltammogram obtained. Figure 9e showing the comparative QV,s of sample at a scan rate of 25 mV $s^{-1}$. While PANI and PANI-AIL showed open-loop QV, PANI-PIL showed closed-loop QV Figure 9b-d.

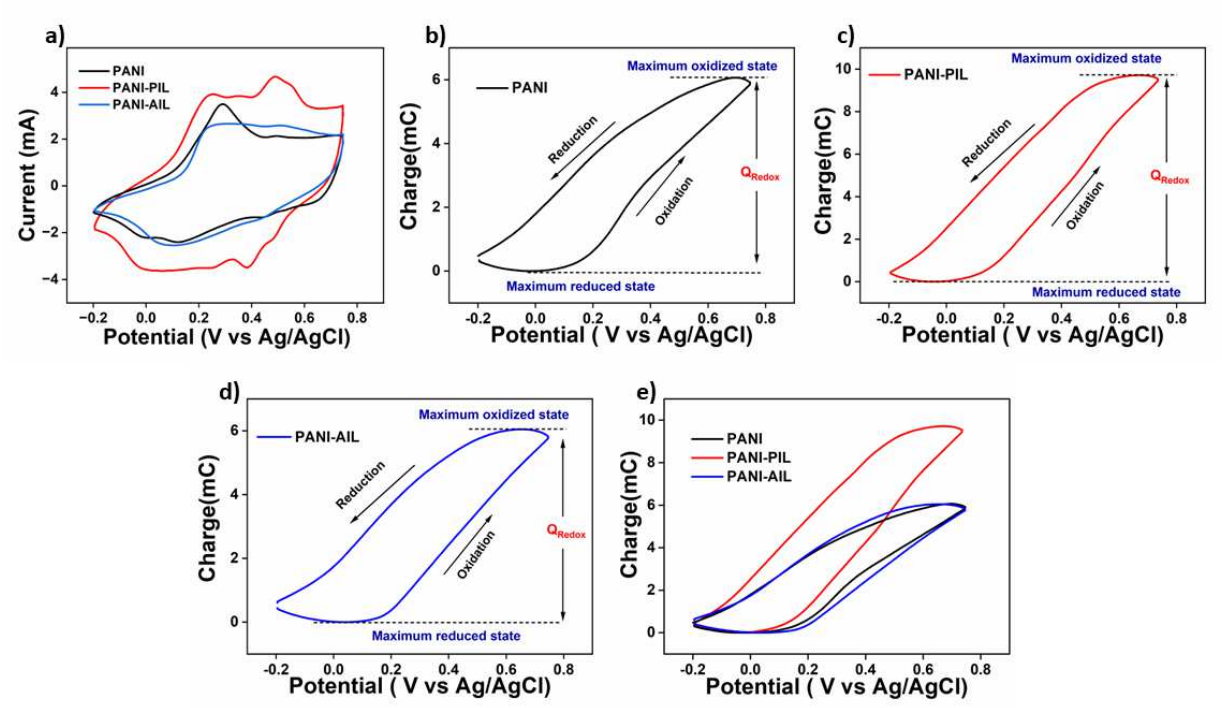



*Figure 9 (a) cyclic voltammograms (CV) of PANI, PANI-PIL, and PANI-AIL at 25 mV $s^{-1}$; 9(b,c,d) corresponding QVs.*

The closed loop indicates a fully reversible redox process, where the oxidation charge equals the reduction charge, confirming the absence of significant parallel irreversible reactions within the investigated potential window. In contrast, an open loop reflects the

irreversible oxidation processes that occurs parallel to the reversible process[37]. The total redox charge of PANI-PIL was obtained from the difference between the maximum and minimum values of the closed loop, demonstrating complete charge balance between oxidation and reduction. Similarly, oxidation charge exceeds the reduction charge, resulting in an open loop. This behaviour indicates the occurrence of irreversible oxidation process. This irreversible oxidation charge is calculated by taking the difference between the charges at the beginning and end of the loop. The reversible charge is then determined by subtracting the irreversible charge from the total charge defined as the difference between QV maxima and QV minima[37, 39]. The electrical charge consumed by the PANI, PANI-PIL, and PANI-AIL at a scan rate of 25 mV $s^{-1}$, was found to be 6.06 mC, 9.7 mC, and 6.04 mC, respectively.

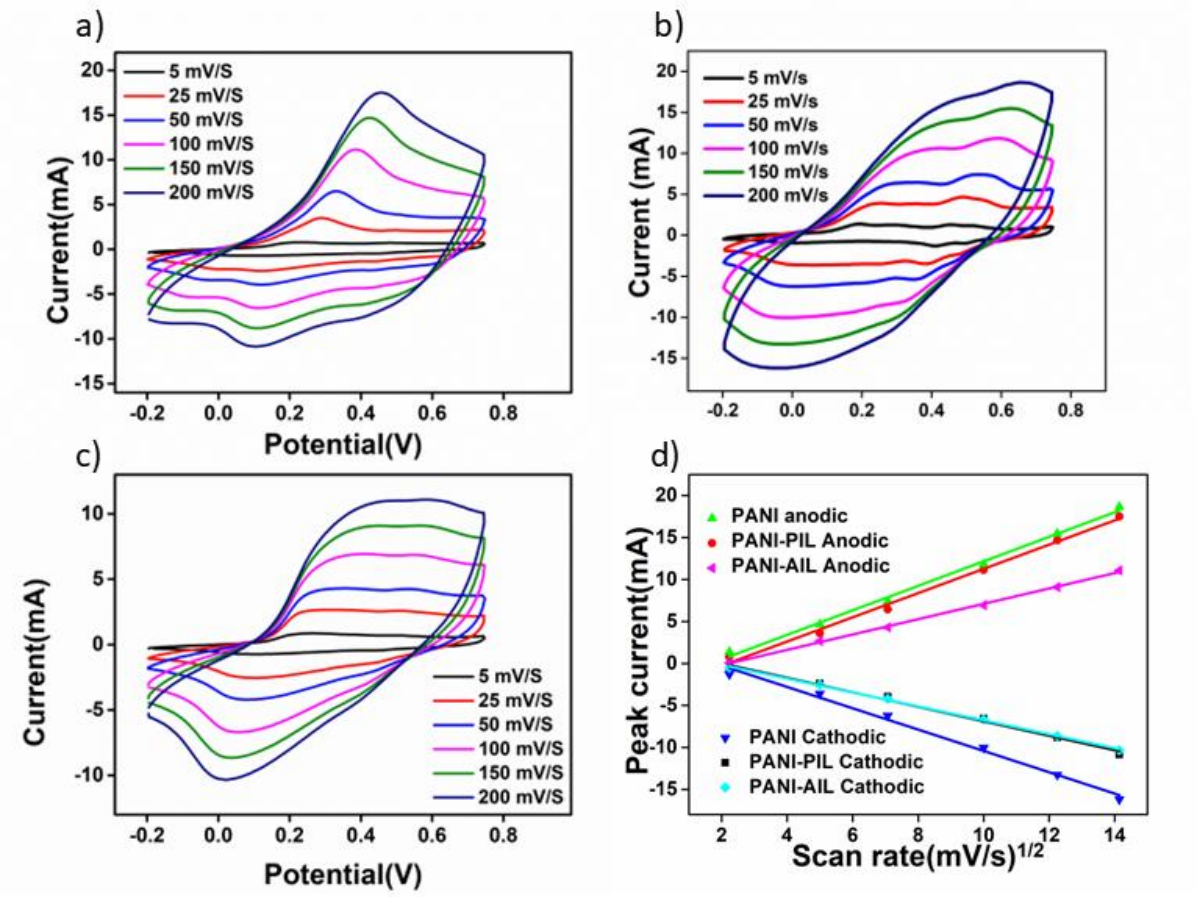



*Figure 10 (a)CV of PANI, b) CV of PANI-PIL, and (c) CV of PANI-AIL at different scan rates. (d) Plot of peak current versus the square root of scan rate showing the diffusion-controlled behavior*

Figure 10(a-c) presents the CVs of PANI, PANI-PIL, and PANI-AIL recorded over a scan rate range of 5-200 mV $s^{-1}$. from the Figure it is clear that the anodic peaks shift toward more positive potentials, while the cathodic peaks move toward more negative potentials with increasing the scan rate, indicating increased resistance to the redox process at higher scan rates. This behavior can be attributed to the limited diffusion of counter ions into and out of the polymer matrix. At lower scan rates, the opposite trend is observed, suggesting improved ion transport facilitated by greater conformational flexibility of the polymer chains. This flexibility allows the formation of additional free volume, enabling accommodation of a larger number of counter ions and solvent molecules. Furthermore, the linear relationship between the peak currents and the square root of the scan rate (Fig. 10d) confirms that the redox processes at the electrode-electrolyte interface are predominantly diffusion-controlled.

### *3.2.2. Reaction-driven sensing characteristics towards their working conditions: voltametric study*

The sensing capability of the PANI, PANI-PIL, PANI-AIL toward its surrounding working conditions was systematically investigated using voltammetric analysis. Stationary CVs were recorded under different environmental working conditions (electrical and chemical). The results demonstrate that the electrical charge consumed during the redox process can serve as a reliable sensing parameter. The redox charge consumed during the reaction was quantified from coulovoltammogram. The relation between the charge and the working variable is explored and established using theoretical equation. this relation reveals that, the consumed redox charge is act as the sensing parameter[12, 40]

#### *3.2.2.1. Sensing electrical working condition- current sensor*

To explore the reactive sensing capability of the polymers towards their electrical conditions, the influence of scan rate on the electrochemical reactions was examined by recording the CVs at different scan rate in 1M $H_2SO_4$ at room temperature (Figure 10 a-c) ). The QVs of each polymer also obtained from their corresponding CVs, shown in Figure 12 and the charge consumed during the reaction was calculated from the QV..

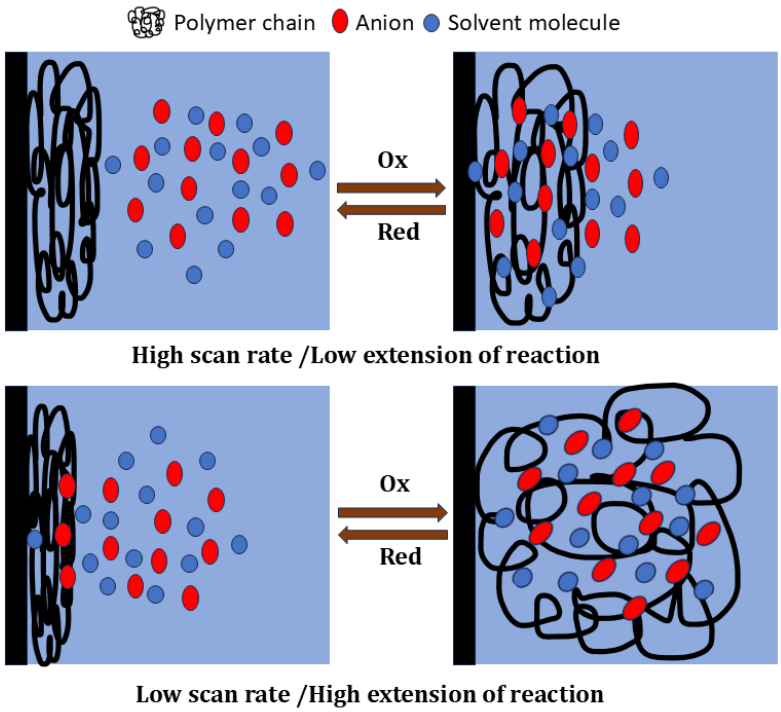



*Figure 11: Schematic representation of extension of reaction at different scan rates.*

The voltammetric responses recorded at different scan rates (10a-10c) revealed that both anodic and cathodic peak currents increase with increasing scan rate, indicating scan-rate-dependent electrochemical kinetics. From Figure 12a to 12c, it can be observed that the charge consumed during the reaction is decreased by increasing the scan rate.A decrease in scan rate results in prolonged reaction time, allowing enhanced exchange of anions and solvent molecules within the polymer matrix. This increased interaction broadens the extension of the redox reaction, leading to higher redox charge consumption[1, 35]. Conversely, at higher scan rates, the reduced reaction time limits ion and solvent exchange, resulting in a smaller reaction extension and lower redox charge consumption. The double logarithmic relationship between scan rate and consumed redox charge, as depicted in Figure 12d-12f, confirms that the PANI-based electrodes effectively sense electrical working conditions by utilizing the consumed redox charge as the sensing parameter. The sensitivities are calculated ,−0.28, −0.29, and −0.28 C $(mV\ s^{-1})^{-1}$ for PANI, PANI-PIL, and PANI-AIL, respectively, with PANI-PIL exhibiting higher sensitivity.

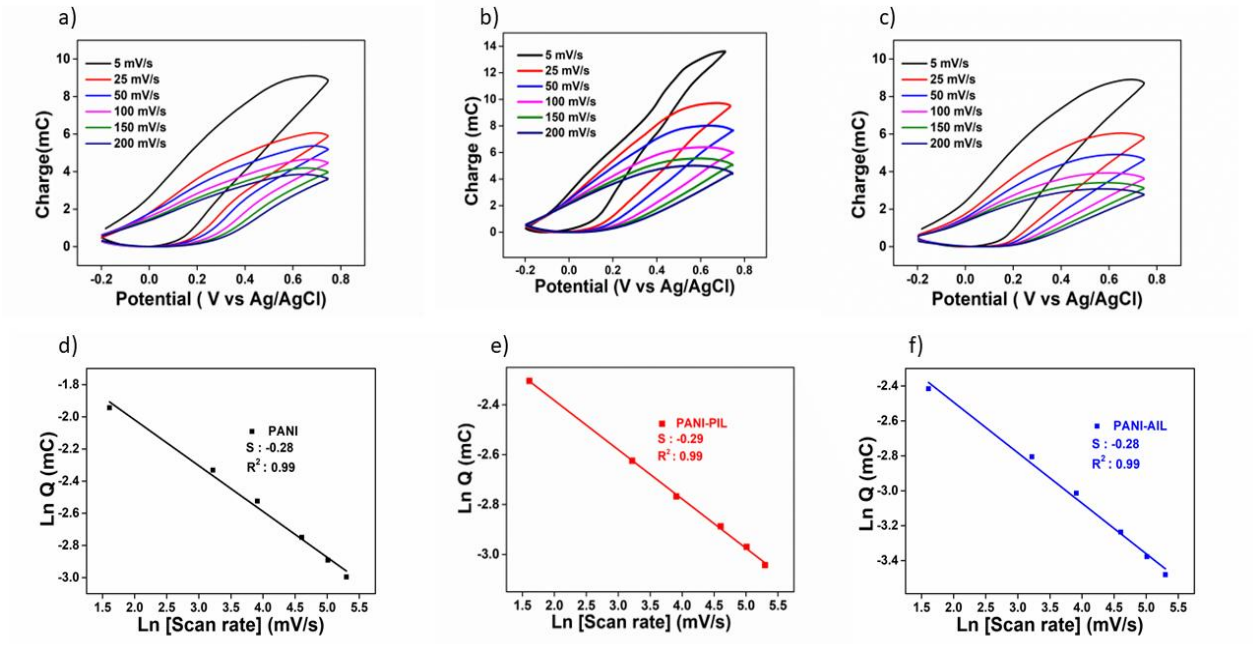



*Figure 12. QVs of (a) PANI, (b) PANI-PIL, and (c) PANI-AIL obtained from CV integration. (d-f) Corresponding linear logarithmic relationships between charge and scan rate (check the captions from other papers).*

***Theoretical description***

The sensing mechanism is governed by the amount of redox charge consumed during the electrochemical reaction, which was quantitatively measured and employed as the key sensing parameter for PANI, PANI-PIL, and PANI-AIL systems. To establish the relationship between the consumed redox charge and the working variables, a detailed investigation is carried out,

$$(PANI^{*})_S + n(A^{-})_{sol} + m(H_2O) \leftrightharpoons [(PANI)^{n+}(A^{-})_n(H_2O)_m]_{gel} + ne^{-} \qquad (1)$$

The reaction rate is expressed as:

$$k[HSO_4{}^{-}]^{\propto}[PANI_0]^{\beta} \qquad (2)$$

where *r* represents the reaction rate and *k* denotes the rate constant. The concentration of the counter anion, sulfate ion, is expressed a $HSO_4{}^{-}$, while $PANI_0$ corresponds to the concentration of the electrochemically active centres within the polymer matrix. The reaction orders with respect to the counter anion and the polymer active centres are

represented by α and β, respectively. Since the volume of the polymeric active centres changes continuously during the redox process, the rate equation is reformulated in terms of the concentration of active centres per unit dry mass of the polymer (specific concentration), thereby expressing the rate as a mass quantity[1].

Reaction (1) describes the variation in the concentration of polymeric active centres, which can be directly evaluated by analysing the redox charge consumed during the electrochemical process.

The change in concentration of polymeric active centres is given by:

$$\bar{r} = \frac{R}{m} = \frac{k}{m}[HSO_4^-]^{\alpha}[PANI_0]^{\beta} \quad (3)$$

The particular reaction rate is defined as:

$$-\Delta[PANI_0] = \frac{Q}{mzF} = \frac{q}{zF} \quad (4)$$

where $q$ denotes the specific charge of the active centres, $Q$ represents the total charge consumed during the redox reaction, $z$ is the valence of the counter anion (for $SO_4^{2-}$, $z$ = 2), and $F$ is the Faraday constant (96489 C $mol^{-1}$).

The relationship between reaction rate and charge consumption is expressed as:

$$r = \frac{\partial[PANI_0]}{\partial t} = \frac{\partial(q)}{\partial t} = \frac{1}{F}\frac{\partial q}{\partial t} \quad (5)$$

The mean specific reaction rate can be obtained from the coulovoltammetric response by calculating the time required to complete a given potential window (ΔE/v), where v is the scan rate.

The mean reaction rate expression is given by:

$$\bar{r} = \frac{\Delta[PANI_0]}{\Delta t} = \frac{q}{Ft} = \frac{qv}{F\Delta E} \quad (6)$$

Rearranging Eqn. (5) yields:

$$[PANI_0] = \frac{Q}{VzF} = \frac{q\rho}{mzF} \quad (7)$$

The consumed redox charge is employed to evaluate the extension of the reaction, where $V$ represents the effective volume of the polymer active centres (L) and $\rho$ denotes the polymer density (g $L^{-1}$). The oxidation or reduction charge determines the change in the concentration of the polymeric active centres. The reaction rate is defined by the rate of change of [PANI] with respect to time, which can be related to the applied potential, scan rate (ν), and time increment ($\partial t = \partial E/\nu$).

The formation of polarons during oxidation corresponds to a decrease in the concentration of neutral polymeric active centres, equivalent to the number of moles of electrons released from the polymer backbone.

Accordingly, the reaction rate can also be expressed as:

$$R = -\frac{\partial[PANI_0]}{\partial t} = \frac{\partial\left(\frac{q\rho}{F}\right)}{\partial t} = \frac{\nu\rho}{F}\frac{\partial q}{\partial E} \quad (8)$$

Which can be further rearranged as:

$$\frac{\nu\rho}{F}\frac{\partial q}{\partial E} = k[Cl^-]^{\propto}[PANI_0]^{\beta} = k[HSO_4{}^-]^{\propto}\left(\frac{q\rho}{F}\right)^{\beta} \quad (9)$$

Rearrangement of the governing equations yields:

$$\frac{1}{q^{\beta}}\frac{\partial q}{\partial E} = \frac{k[HSO_4{}^-]^{\propto}\mathrm{F}^{1-\beta}}{\rho^{1-\beta}}\frac{1}{\nu} \quad (10)$$

Integration of the left-hand side is carried out for the reversible coulovoltammetric charge from zero charge to the maximum reversible charge ($q^{R}$), while the right-hand side is integrated from the initial potential ($E_o$) to the potential corresponding to the maximum charge ($E^{R}$).

The integrated form of the equation is:

$$\int_{0}^{qR} \frac{1}{q^{\beta}} \partial q = \int_{E0}^{ER} \frac{k[HSO_4^-]^{\propto} F^{1-\beta}}{\rho^{1-\beta}} \frac{1}{\nu} \partial E \quad (11)$$

Which simplifies to:

$$q_R^{1-\beta} = \underbrace{\frac{(1-\beta)k[HSO_4^-]^{\propto} F^{1-\beta} \Delta E}{\rho^{1-\beta}}}_{h'} \frac{1}{\nu} \quad (12)$$

The degree of the electrochemical reaction is therefore directly determined by the amount of redox charge consumed during the process. When experimental parameters such as electrolyte concentration, working temperature, atmospheric pressure, and potential window are maintained constant, the reaction extension—and hence the consumed redox charge—decreases with increasing scan rate. The constant terms in Eqn. (13) can be combined into a single constant (*h'*). Taking the natural logarithm of both sides yields:

$$lnq_r = x - y \ln \nu \quad (13)$$

The double logarithmic relationship provides the sensitivity (*y*) and the intercept (*x*) of the linear fit.

The expressions for the intercept and sensitivity are given by:

$$x = \frac{\ln h'}{1-\beta} \quad (14)$$

$$y = \frac{1}{1-\beta} \quad (15)$$

The sensing Eqn.15 establishes a direct relationship between the reaction extension and the scan rate, enabling the assessment of electrical working conditions through the conformational response of the polymer chains within the electrode film. This behaviour highlights the biomimetic nature of the PANI-based electrodes[12].

Using Equation 15, fitting analysis was performed on the experimental results. The slope of the linear fit represents the sensitivity of the system and reflects the rate at

which the consumed redox charge decreases with increasing scan rate. At lower scan rates, extended reaction times allow significant conformational rearrangements of the polymer chains, facilitating enhanced diffusion of sulfate ions and solvent molecules within the polymer matrix. This leads to increased redox charge consumption.

On the other hand limited reaction duration at higher scan rates restricts ion transport and polymer chain relaxing, which reduces reaction extension and redox charge consumption. These findings suggest that with greater sweep rates, the macromolecular structural dynamics become more limited,resulting in decreased redox activity.

The experimental and theoretical data confirms that PANI-based electrodes effectively sense electrical working conditions by utilizing the consumed redox charge as the sensing parameter. Among the investigated electrodes, PANI-PIL exhibits superior sensing performance due to its enhanced conformational changes during electrochemical cycling

***3.2.2.2. Sensing chemical working condition - concentration sensor.***

To explore the reactive sensing ability of the polymers towards their chemical working condition, CV was carried out in different concentrations of aq. $H_2SO_4$ solutions at the scan rate of 25 mVs-1 at room temperature. The resulting CVs are shown in Figure 13a, 13d, and 13g. The CV exhibits well-defined redox characteristics, with both anodic and cathodic peak current increasing as the electrolyte concentration rises. This behaviour reveals the enhanced ionic mobility and charge compensation process at higher proton concentrations, whereas a noticeable decline is observed at lower concentrations. At higher concentrations, the polymer backbone undergoes oxidation, which promotes greater intercalation of counter anions and solvent molecules into the polymer matrix, thereby enhancing the electrochemical redox charge consumption. In contrast, at lower concentrations, the extension of oxidation is limited, resulting in reduced free volume and consequently lower charge consumption during the redox process.

The relationship between electrolyte concentration and consumed redox charge showing a linear relation with high correlation coefficients ($R^2$ = 0.99), as shown in Figures 13c, 13f, and 13i. This indicates a consistent increase of charge consumption

with electrolyte concentration. The slope (S) gives the sensitivity of the material towards the variations in electrolyte concentrations. Among the studied materials, PANI and PANI-AIL show similar sensitivities (S = 0.101), while PANI-PIL exhibits a slightly higher sensitivity (S = 0.124), indicating enhanced responsiveness. The extension of the redox reaction increases with electrolyte concentration, leading to more pronounced conformational changes and structural variations within the polymer chains. This behaviour highlights the ability of these materials respond to or sense their chemical environment through changes in consumed electrical charge, making them promising candidates for sensing applications.

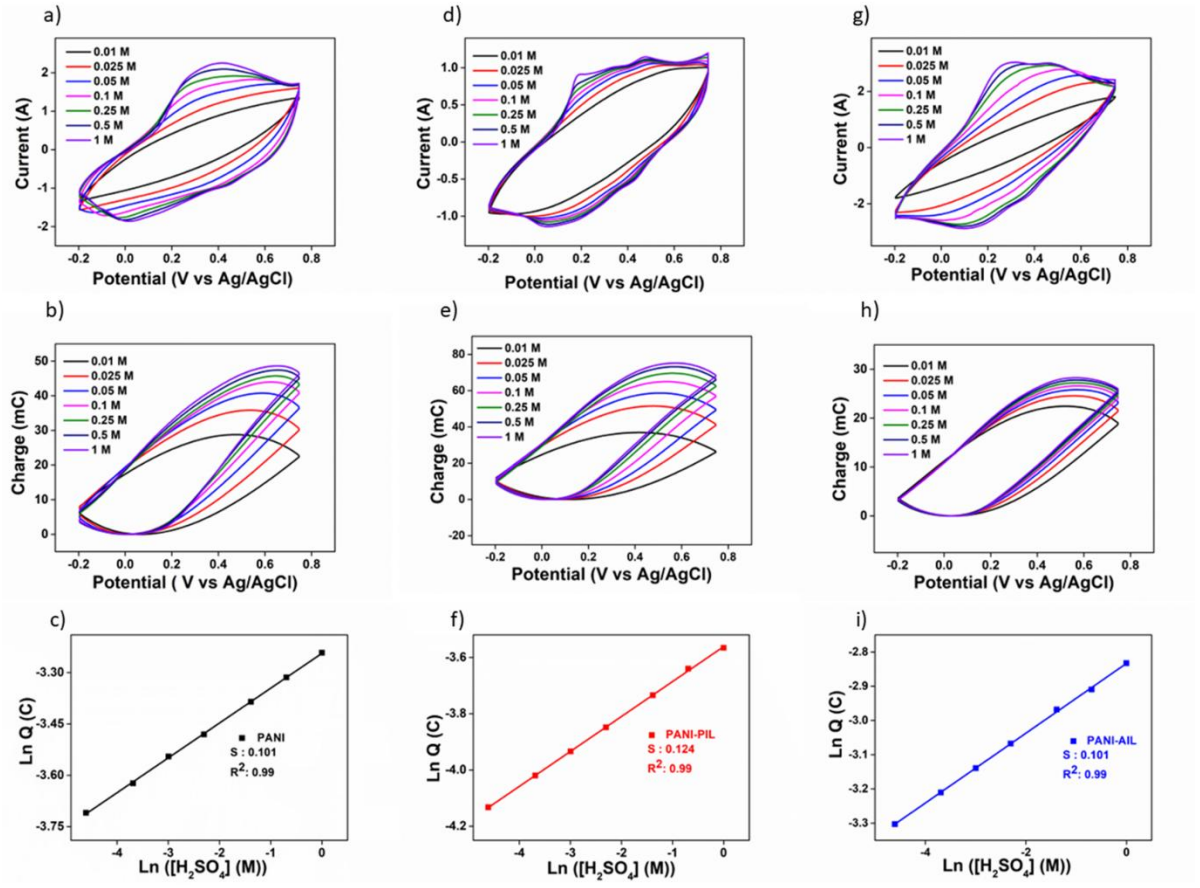



*Figure 13: Cyclic voltammograms of a) PANI, d) PANI-PIL , g) PANI-AIL obtained in different concentrations of aqueous solution of $H_2SO_4$ between -0.2 V to 0.75V at a scan rate of 25 mV $s^{-1}$. (b,e,h) corresponding Coulovoltammogram obtained by integrating*

*the voltammograms obtained in (a,d,g). (c,f,i) Double logarithmic relation of the charge consumed during the redox reaction of polymer sample with the electrolyte concentration of aqueous $H_2SO_4$.*

***Theoretical description***

Equation (6) provides an alternative formulation for describing the average reaction rate of the PANI-based electrodes.

$$\frac{qv}{F\Delta E} = \frac{k}{m}[HSO_4{}^-]^{\alpha}[PANI_0]^{\beta} = \frac{k}{m}[HSO_4{}^-]^{\alpha}\left(\frac{q}{F}\right)^{\beta} \quad (16)$$

By rearranging Eqn. (16), Eqn. (17) is obtained, which establishes a relationship between the change in electrolyte concentration and the amount of redox charge consumed during the electrochemical reaction.

$$q^{1-\beta} = \underbrace{\frac{k\Delta E F^{1-\beta}}{v}}_{k'}[HSO_4{}^-]^{\alpha} \quad (17)$$

The coefficients appearing in Eqn. (17) are combined into a single constant, denoted as k′. Upon taking the natural logarithm of Eqn. (18), a double-logarithmic relationship is obtained, correlating the redox charge consumed during the reaction—under constant pressure, temperature, potential window, and scan rate—with the electrolyte concentration.

$$\boldsymbol{l}n(q) = a + bln[HSO_4{}^-] \quad (18)$$

Eqn. (18) describes a direct relationship between the consumed redox charge (q) and the sulfate ion concentration, $[HSO_4{}^-]$, where the intercept of the linear fit is represented by a and the slope by b.

$$a = \frac{lnk'}{1-\beta} \quad (19)$$

$$b = \frac{\alpha}{1-\beta} \quad (20)$$

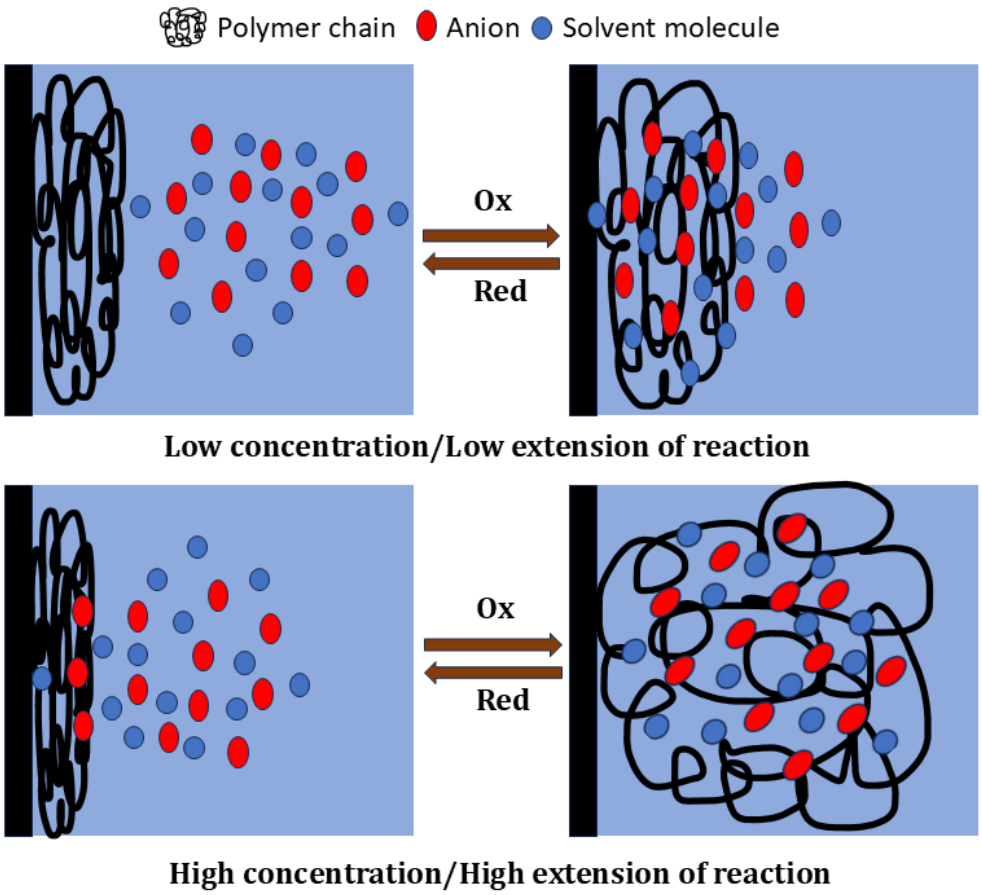



*Figure 14: Schematic representation of extension of reaction at different concentration of $H_2SO_4$.*

The experimental results obtained for PANI, PANI-PIL, and PANI-AIL electrodes, as shown in Fig. 13(c,f,i), exhibit excellent agreement with the theoretical model described by Eqn. (19). The consumed electrical charge during the redox reactions of material senses the working chemical condition. The sensing behaviour of these polymeric systems originates from reaction-induced conformational rearrangements of the polymer chains, which are modulated by changes in the electrolyte concentration. The polymer chain was fully oxidized at higher concentrations in the same potential window because, the available chemical energy is large for higher concentrations. The large free volume generated by this complete oxidation drives the intercalation of the counter anions and water molecules from the electrolyte to the polymer matrix. At lower concentrations, the available chemical energy is low, and partial oxidation of the polymer chain takes place which generates a low amount of free volume to enter/expel

the counter anions and solvent molecules during the oxidation and reduction This response closely resembles the functioning of biological muscles, where chemical variations induce structural motion that conveys information regarding the surrounding environment[35, 37]. Consequently, the PANI-based electrodes demonstrate biomimetic sensing characteristics, enabling the detection of chemical working conditions through variations in consumed redox charge (figure 14).

### 3.2.3 Reactive sensing characteristics: Chronopotentiometric response

The biomimetic reactive sensing behavior of PANI, PANI-PIL, and PANI-AIL toward their working environment was investigated using chronopotentiometry. Under galvanostatic conditions, a constant current (either anodic or cathodic) was applied to control the reaction rate, induce a controlled shift in polymer composition, and monitor the evolution of the material potential during redox processes. The chronopotentiometric responses were recorded and analyzed to evaluate the dynamic behavior of the polymer systems.Any physical or chemical variable affecting the electrode reaction rate was found to directly influence the potential evolution of the polymer chains. To assess the sensing capability under different environmental conditions, the samples were subjected to consecutive square current waves, enabling the study of electrical (applied current), and chemical (electrolyte concentration)variables. Prior to chronopotentiometric measurements, the materials were electrochemically stabilized by recording 20 consecutive cyclic voltammograms to ensure reproducible behavior. The application of consecutive square current pulses generated well-defined chronopotentiometric responses under constant charge conditions. Variations in the studied environmental parameters produced measurable changes in the potential evolution of the materials during the redox reaction, confirming their ability to function as reactive electrochemical sensors[12, 37].

#### *3.2.5 Sensing working electrical condition: Current sensor*

Electrochemical redox reactions of PANI involve anodic and cathodic reactions, consisting of anodic oxidation of polymer chains with intercalation of counterions from

the electrolyte ($HSO_4^-$) and water molecules. Cathodic reaction involves the reverse process, the reaction represented as

$$[PANIH^*] + xA^- + y(H_2O) \rightleftharpoons (\mathrm{PANI})^{X+}(A^-)y(H_20)_K + H^+ + (x+y)e^- \quad (21)$$

Where ( $A^-$) represents the anions exchanged for electrical neutrality, and the $H^+$ denotes the proton released during the reaction. The involvement of solvated ions and water molecules ($H_2O$) balances the osmotic pressure through ion-solvent exchange, leading to the formation of a dense polymeric gel structure. During this reaction, the polymer undergoes **n** consecutive redox steps, resulting in compositional changes that contribute to both actuating and self-sensing functionalities of PANI.

$$E = E_0 - \frac{RT}{nF} \ln\left(\frac{[A^-][PANIH^*]}{[H^+][(PANI)^{X+}(A^-)y(H_20)_K]}\right) \quad (22)$$

Here E and $E_0$ represents the electrode and standard electrode potential, R is the universal gas constant ( R=8.31J/K mol ),F is the Faraday constant ( F= 96485 C/mol ) Here, $[A^-]$is the concentration of the counter anions in solution, $[PANIH^*]$denotes the concentration of the active protonated centers, while $[H^+][(PANI)^{X+}(A^-)y(H_20)_K]$ represents the oxidized PANI complex stabilized by anions and solvated water molecules and n is the number of electrons transferred in the redox process, and the rate of the reaction is expressed as,

$$r = k\,[PANIH^*]^{a-}[A]^b[H^+]^c \quad (23)$$

Here, r represents the reaction rate, k is the kinetic constant, and aaa, bbb, and ccc denote the reaction orders corresponding to the polymer's active centers, the anion/electrolyte concentration, and the solution pH, respectively. The process proceeds via proton elimination through several energetic steps, each accompanied by the removal of a single electron.The relationship between the current and the rate of reaction, which can be expressed as follows, is obtained by a constant current flowing through the PANI electrode material. $r = \frac{q}{FV} = \frac{it}{FV} \leftrightarrow i = \frac{rFV}{t}$ (24)

where q is the charge, i is the current, t is the duration of current flow, F is the Faraday constant, and V is the film volume. The Butler-Volmer equation for electrochemical kinetics was employed to establish the relationship between the rate constant and the potential variation during the redox (anodic or cathodic) process.

$$i_a = FVk_{\alpha}\left[PANIH_p\right]^a[A^-]^b[H^+]^c \quad (25)$$

$$i_a = FVk_{a0}\left[PANIH_p\right]^a[A^-]^b\,[H^+]^c exp\left(\frac{(1-a)nF(E-E_0)}{RT}\right) \quad (26)$$

In this case, the evolved potential during the reaction is obtained as a function of the electrolyte concentration, applied current, and reaction temperature. Consequently, the potential developed in the system depends on these parameters and can be expressed as:

$$E_a = E_0 + \frac{RT}{(1-a)nF}\left(ln\left(\frac{i_a}{FV}\right) - b\,ln[A^-] - a\,ln\left[PANIH_p\right] - cpH - ln\,k_{a0}\right) \quad (27)$$

This provides insight into the sensing behavior of PANI during the anodic process. The oxidation of the material occurs through n consecutive steps, and the overall process can be represented by the general equation:

$$E_n(t) = E_0 + i_aZ + (n-1)\Delta E + \frac{RT}{(1-a)F} \times$$

$$\begin{Bmatrix} ln\left(\frac{i_a}{FV}\right) - b\,ln[A^-] \\ -a\,ln\left(\left[PANIH_p\right]_{initial} - cpH - \frac{i_at}{FV}\right) - ln\,k_{a0} \end{Bmatrix} \quad (28)$$

where Z represents the impedance of the system, and ΔE denotes the potential difference between the extraction of the last (n-1) electron from the polymer chains (during oxidation) and the first n electron extracted. A similar expression can be derived for the cathodic process. The electrical energy consumed during these redox reactions is governed by the flowing current,electrolyte concentration and the potential evolution, expressed as

$$\mathrm{U} = \mathrm{I}\int \mathrm{Edt} \quad (29)$$

Therefore, as indicated in Eq. (28), when all other variables remain constant, the linear dependence of the evolved electrical energy on a single variable can be used to detect variations in that experimental parameter.

Equation (22) thus relates the electrode potential with the analyte concentration, serving as the fundamental principle for potentiometric-type sensors. According to the Le Chatelier principle, any fluctuation in concentration or solvent environment shifts the equilibrium in order to counter the disturbance, thereby altering both the equilibrium potential and the kinetics of the forward and backward reactions. However, conducting polymers undergo electrochemical redox reactions under non-equilibrium conditions, deviating from the classical Le Chatelier principle. To account for this behavior, Otero et al. redefined the principle, stating that "***any chemical or physical variable that alters the rate of a chemical reaction will redirect the reaction energy to satisfy the imposed energetic demands***". In this framework, the electrochemical potential of the material is highly responsive to external variables that influence the energetic environment of the reaction[2].

Chronopotentiometric (CP) measurements were carried out to evaluate the current-sensing ability of PANI, PANI-PIL, and PANI-AIL in 1 M $H_2SO_4$ electrolyte at room temperature. Successive anodic and cathodic square current pulses (±0.1 to ±1 mA) were applied while maintaining a constant total charge (q = it). The consumption of electrical energy during the redox reaction is calculated using the equation (29),

The resulting chronopotentiograms *(Figure 15 )* show that the potential shifted to more positive values with increasing anodic current *(Figure 15 a,d,g )* and to more negative values with increasing cathodic current*(Figure 15 b,e,h )*. The electrical energy consumed during the redox process, taken as the sensing parameter, exhibited a linear dependence on both anodic and cathodic currents, confirming the ability of the materials to sense the applied current. The sensitivity of the samples followed the order PANI-PIL < PANI < PANI-AIL, with cathodic sensitivities of -1.01, -0.76, and -0.55 $mJmA^{-1}$ and anodic sensitivities of 0.93, 0.78, and 0.54 $mJmA^{-1}$, respectively.

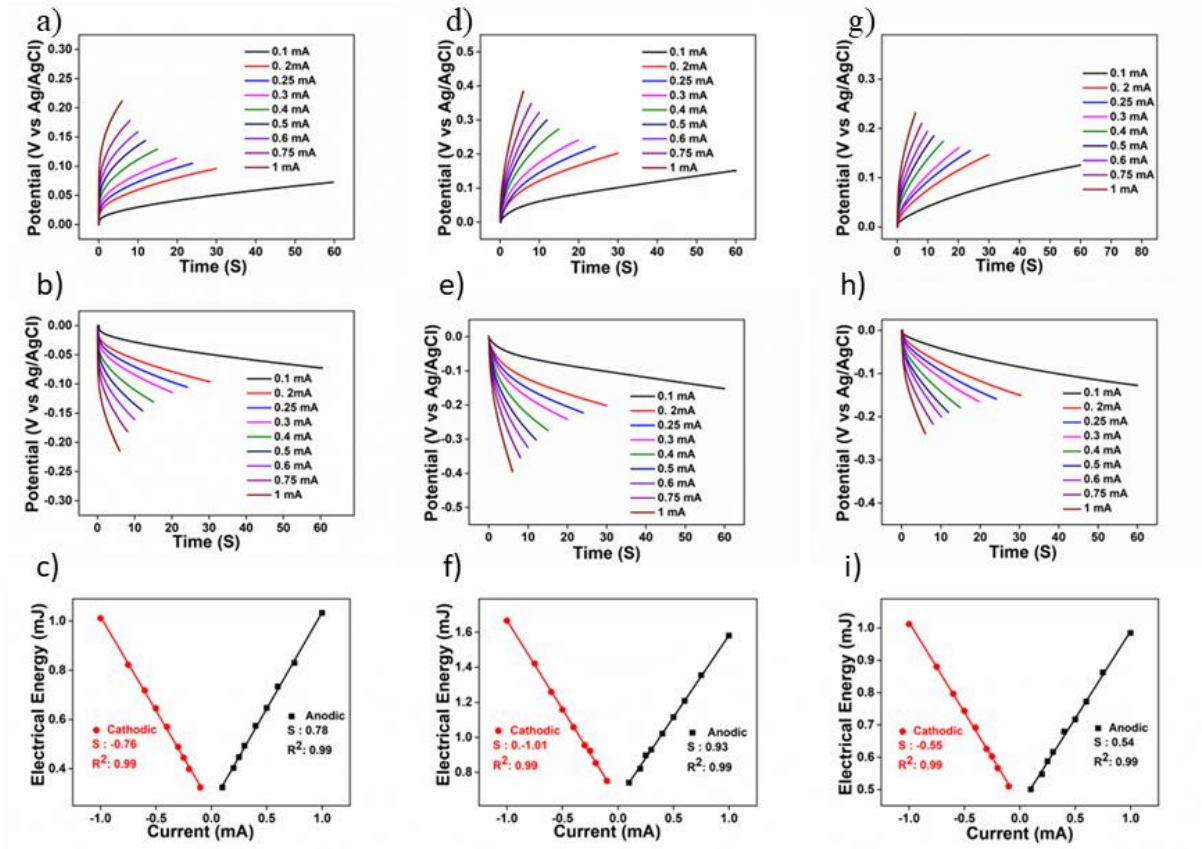



*Figure 15 Chronopotentiograms recorded for different concentrations of $H_2SO_4$ when currents of 0.1 mA and −0.1 mA were applied for 60 s.(a,b) PANI, (d,e) PANI-PIL, and (g,h) PANI-AIL .(c,f,i) Electrical energy (U) consumed by the film during the reaction as a logarithmic function of electrolyte concentration at room temperature.*

### *3.2.6 Sensing working chemical condition: Concentration sensor*

The results of chronopotentiometry experiments conducted on PANI, PANI-PIL, and PANI-AIL electrode materials using varying concentrations of $H_2SO_4$ electrolyte (0.01 M to 1 M) are shown in *Figure 16*. The experiments were performed by applying a constant charge of 6 mC at room temperature, with a fixed anodic current of 0.1 mA during oxidation and a cathodic current of -0.1 mA during reduction, each maintained for 60 seconds. As shown in Figure 16(a,d,g) higher electrolyte concentrations promote faster reaction kinetics and lower interfacial resistance, leading to smaller potential differences during constant current operation. Conversely, lower electrolyte concentration increase ionic resistance, resulting in larger potential differences.

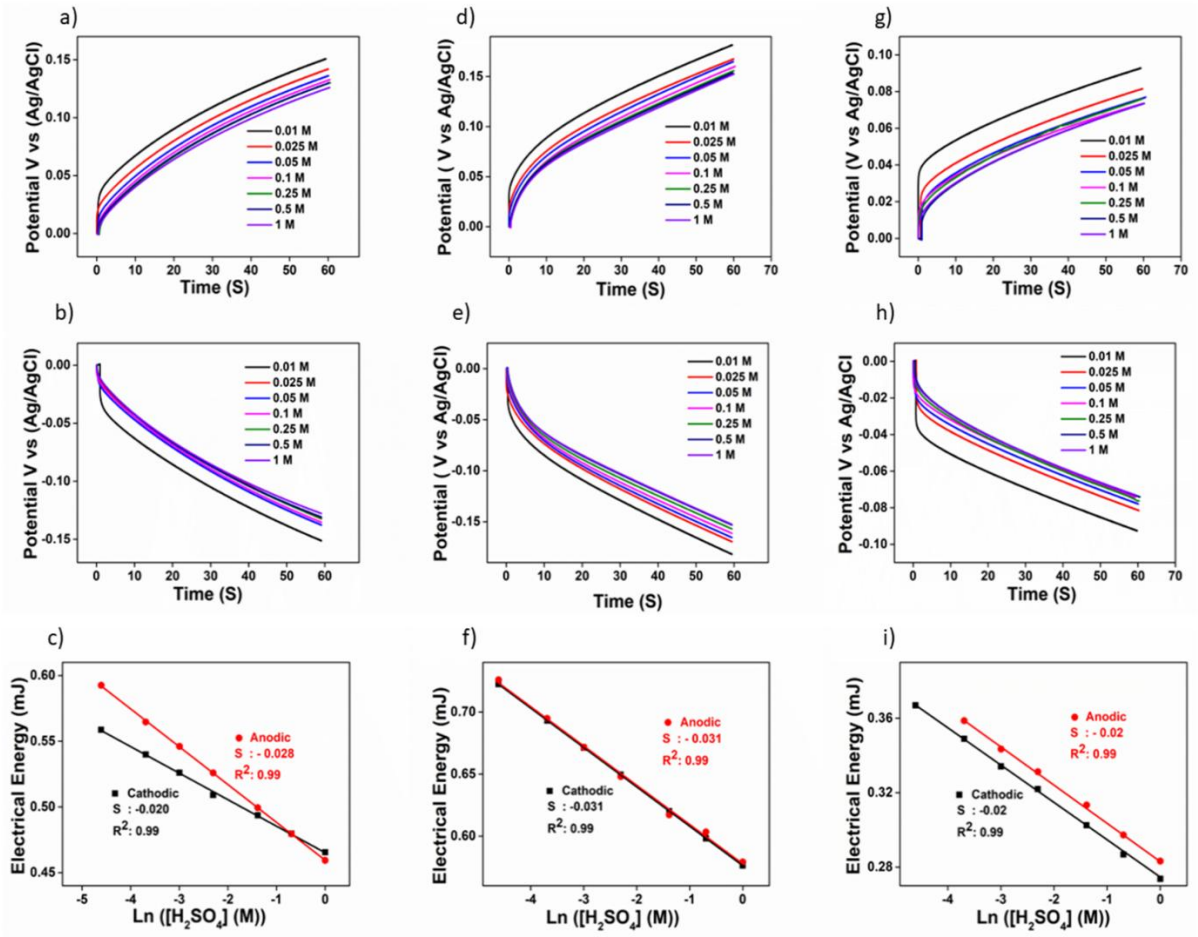



*Figure 16 Chronopotentiograms obtained when different constant (a) anodic and (b) cathodic currents were applied to polymer sample by passing a constant charge of 6 mC in 1 M $H_2SO_4$ solution (c) electrical energy consumed by the film as a function of applied current ($R_2$ is the correlation factor).*

The electrical energy consumed during the redox processes, obtained by integrating the CP curves, acts as the sensing parameter for electrolyte concentration. The electrical energy consumed during the reaction senses the chemical working conditions.The energy response exhibits a semi-logarithmic dependence on concentration, demonstrating the materials' capability to detect electrolyte variations effectively. Moreover, consistent with the behavior of conducting polymer electrodes, the oxidation and reduction processes are energetically asymmetric, consuming different amounts of energy depending on the electrolyte concentration.The sensitivity of the samples

followed the order PANI-PIL < PANI < PANI-AIL, with cathodic sensitivities of -0.031, -0.028, and -0.02 $M^{-1}$ and anodic sensitivities of 0.031, 0.028, and 0.02 $M^{-1}$, respectively.

### *3.3 Supercapacitive studies*

Supercapacitors are promising electrochemical energy storage devices that have gained considerable attention due to their fast charge discharge capability , excellent cyclic stability and power density. They store energy through electrostatic charge accumulation at the electrode electrolyte interface ie, electrical double layer capacitance, through fast and reversible redox reaction pseudocapacitance. Polyaniline have been widely explored as electrode materials because of their high conductivity and enhanced charge storage through doping and dedoping mechanisms[41].

The GCD profiles of PANI, PANI-PIL, PANI-AIL were measured in a potential window of -0.2 V to 0.75V and a current density varying from 0.5 $Ag^{-1}$ to 5 $Ag^{-1}$. The results of the GCD are shown in *figure 17*. The findings show a nearly triangular GCD curve with very less IR drop indicating that the material have a huge potential to be used as an electrode material for the supercapacitor device. The capacitance of the PANI, PANI-AIL, and PANI_PIL were also calculated from the GCD and found to be 277 $Fg^{-1}$, 174 $Fg^{-1}$, and 249 $Fg^{-1}$ respectively. The results indicate that the PANI prepared from protic ionic liquid show superior properties than the PANI prepared from aprotic ionic liquid. The capacitive retention of the material was also calculated and found to be 49.1%, 45.5%, and 60.9% for PANI, PANI-AIL, and PANI-PIL respectively. Greater retention percentage indicates that the PANI doped with protic ionic liquid is suitable for energy storage applications.

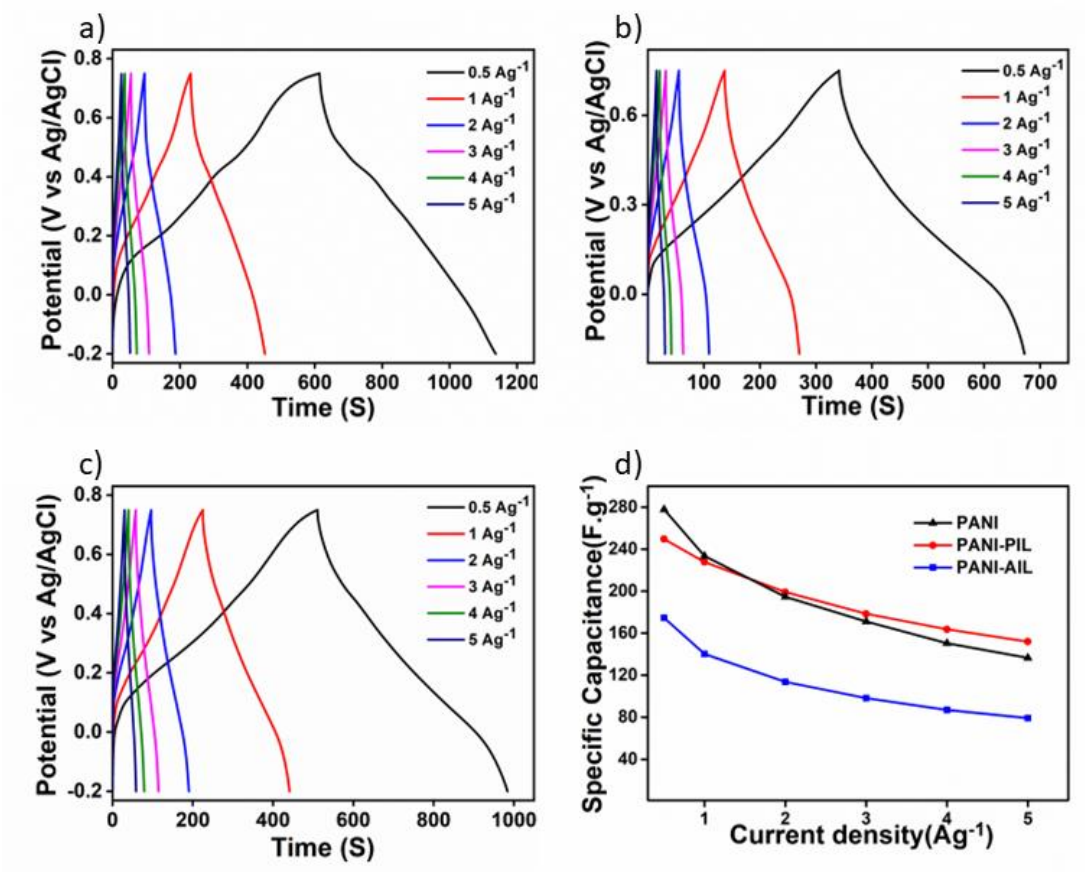



*Figure 17: GCD curves of a) PANI, b) PANI-AIL, c) PANI-PIL and d) capacitance calculated from GCD curve.*

Figure 18 shows the specific capacitance retention of PANI, PANI-PIL, and PANI-AIL over 3000 cycles. PANI-PIL exhibits the highest stability, with only a slight decrease in capacitance 73.35 % , indicating good durability. PANI also maintains good cyclic stability after 3000 cycles 70% , showing reliable performance. In contrast, PANI-AIL displayed a notable drop in capacitance 55.6% , suggesting lower stability and making it less suitable for long-term energy storage compared to PANI and PANI-PIL. [41, 42][42, 43][42, 43].

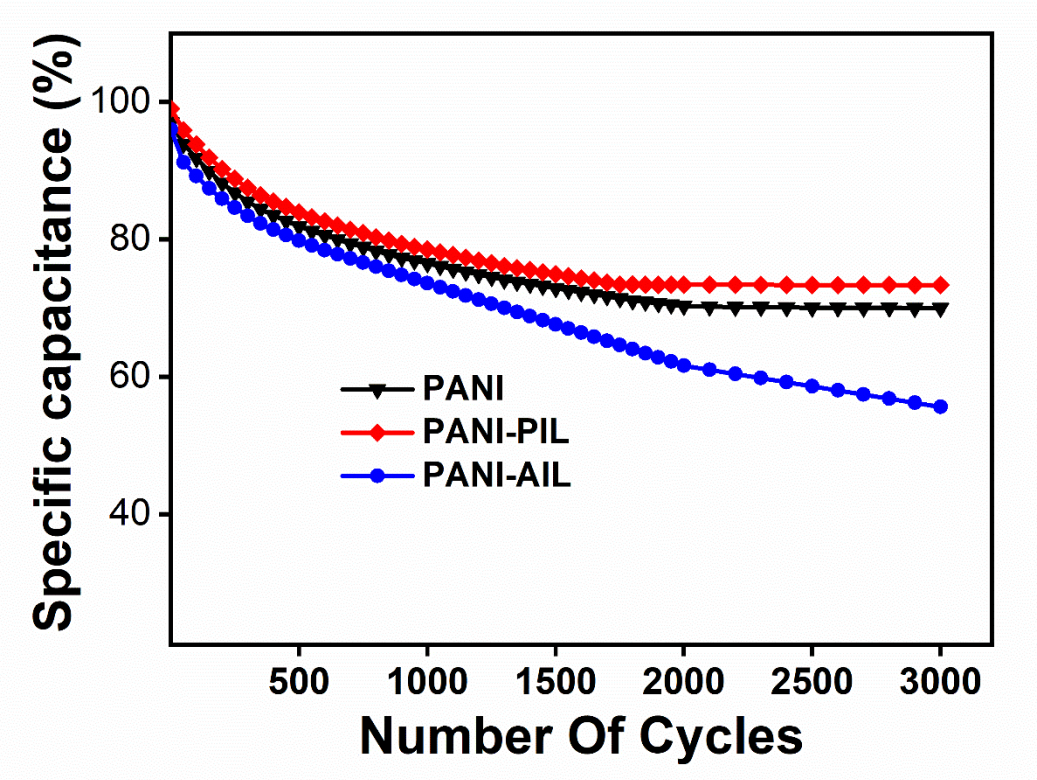



*Figure 18: Capacitance retention of PANI, PANI-PIL, PANI-AIL*

### *3.4 Electrochemical Impedance Spectroscopy*

For a journal paper, you can make it more natural and readable like this:

Electrochemical impedance spectroscopy (EIS) measurements were performed over a frequency range of 0.1 Hz to 100 kHz with a sinusoidal perturbation amplitude of 10 mV. The Nyquist plots of PANI-PIL, PANI, and PANI-AIL are shown in Fig. 19. All three samples were successfully fitted using the same equivalent circuit model, R(Q(R(Q(RW)))), which includes solution resistance (Rs), constant phase elements (Q), charge transfer resistance (Rct), and Warburg impedance (W). The similar circuit response indicates that the samples follow a comparable electrochemical mechanism involving interfacial charge transfer, capacitive behavior, and ion diffusion processes [41]. The extracted fitting parameters are summarized in Table 1.

| Parameter | PANI | PANI-PIL | PANI-AIL |
|---|---|---|---|
| Equivalent Circuit | R(Q(R(Q(RW)))) | R(Q(R(Q(RW)))) | R(Q(R(Q(RW)))) |

| | | | |
|---|---|---|---|
| Rs (Ω cm²) | ~1.15 | ~1.09 | ~1.33 |
| Rct (Ω cm²) | ~6.15 | ~6.13 | ~6.154 |
| $CPE_1$ ($Q_1$) | 0.086 | $2.45 \times 10^{-4}$ | $9.36 \times 10^{-4}$ |
| $n_1$ (CPE) | ~0.68 | ~0.79 | ~0.64 |
| $CPE_2$ ($Q_2$) | 0.0145 | 0.0145 | 0.0145 |
| $n_2$ (CPE) | ~0.63 | ~0.65 | ~0.63 |
| Warburg (W) | ~0.0370 | ~0.023 | ~0.0376 |

A comparative analysis of the EIS parameters reveals differences in the electrochemical behavior of the samples. PANI-PIL shows the lowest solution resistance (Rs ≈ 1.09 Ω cm²), indicating improved ionic conductivity and electrolyte accessibility compared with PANI (~1.15 Ω cm²) and PANI-AIL (~1.33 Ω cm²). The similar charge transfer resistance values (~6.13–6.15 Ω cm²) suggest that interfacial electron transfer kinetics remain nearly unchanged among the samples.[2, 43, 44]. Therefore, the variation in electrochemical performance is primarily governed by capacitive and diffusion-related properties[45].

The CPE parameters indicate improved surface characteristics for PANI-PIL, which exhibits the highest $n_1$ value (~0.79), suggesting more ideal capacitive behavior and a more uniform surface compared with PANI (~0.68) and PANI-AIL (~0.64). The lower Warburg coefficient of PANI-PIL (W ≈ 0.023) confirms faster ion diffusion, while PANI and PANI-AIL show slower ion transport. Overall, PANI-PIL exhibits enhanced capacitive behavior and ion transport, supporting its higher capacitance and improved cycling performance.

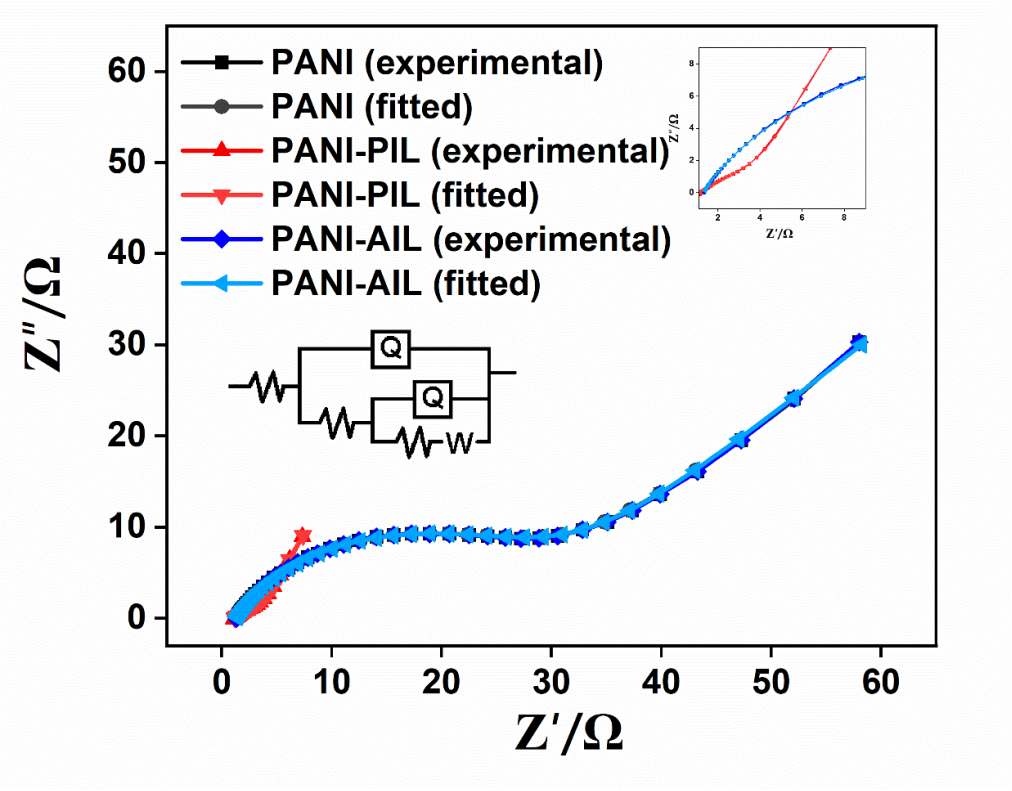



*Figure 19: Nyquist plots of PANI, PANI-PIL, and PANI-AIL electrodes; inset shows the high-frequency region, and the equivalent circuit is included within the figure.*

**Conclusion**

Polyanilines using $H_2SO_4$, a protic ionic liquid, and an aprotic ionic liquid as dopants were successfully prepared via chemical oxidative polymerization. A comparative investigation was carried out to evaluate the influence of conventional acid and ionic liquid dopants on the structural, electrical, and electrochemical properties of the resulting polyaniline materials. The synthesized materials were characterized using FTIR, UV-Visible spectroscopy, TGA, XRD, SEM, contact angle measurements, conductivity analysis, cyclic voltammetry, galvanostatic charge-discharge, chronopotentiometry, and electrochemical impedance spectroscopy.

The results confirmed the successful incorporation of ionic liquids into the polyaniline matrix. UV-Visible spectroscopic studies revealed that the incorporation of the protic ionic liquid reduced the optical band gap of polyaniline, whereas the aprotic ionic liquid caused a slight increase. This reduction in band gap for PANI-PIL suggests enhanced charge delocalization within the polymer backbone, leading to improved electronic

conductivity. Contact angle measurements further showed that PANI-PIL possesses better wettability than pristine PANI and PANI-AIL, facilitating easier electrolyte penetration into the electrode surface. Consistent with these observations, PANI-PIL exhibited the highest electrical conductivity, reaching the order of $10^{-2}$ S $cm^{-1}$.

The electrochemical behavior of the materials was evaluated using CV, CP and GCD studies. The charge consumed during the redox process, which reflects the extent of electrochemical activity, was determined from the QV responses. Among the three samples, PANI-PIL exhibited the highest reversible redox charge (9.7 mC at 25 mV $s^{-1}$), significantly higher than that of pristine PANI (6.06 mC) and PANI-AIL (6.04 mC). These results indicate that the protic ionic liquid promotes more efficient and reversible redox reactions within the conducting polymer matrix. The influence of electrical energetic condition and electrolyte concentration on the electrochemical response revealed that PANI-PIL consistently showed greater sensitivity under varying operating conditions. Chronopotentiometric studies further confirmed its superior anodic and cathodic sensitivities, demonstrating efficient charge storage and discharge during electrochemical cycling.

The supercapacitive performance of the synthesized materials was assessed through galvanostatic charge–discharge measurements. PANI-PIL exhibited a high specific capacitance of 249 F $g^{-1}$ and retained 73.35% of its initial capacitance after prolonged cycling. Although pristine PANI displayed a slightly higher initial capacitance (277 F $g^{-1}$), its lower capacitance retention indicates reduced long-term stability. In comparison, PANI-AIL showed lower capacitance and poorer cycling performance. The improved retention observed for PANI-PIL suggests that the protic ionic liquid contributes to maintaining the structural stability of the polymer during repeated charge-discharge processes.

Electrochemical impedance spectroscopy confirmed similar charge storage mechanisms for all samples through the fitted equivalent circuit model R(Q(R(Q(RW))). PANI-PIL exhibited lower solution resistance, higher CPE exponent, and lower Warburg coefficient, indicating improved ionic conductivity, surface homogeneity, and faster ion diffusion. The similar charge-transfer resistance values

suggest that the enhanced performance of PANI-PIL mainly arises from improved capacitive behavior and ion transport.

Thus, the incorporation of a protic ionic liquid significantly improves the overall performance of polyaniline by enhancing its conductivity, wettability, electrochemical reversibility, ion transport, and cycling stability. The combined effects of these improvements result in superior charge storage and sensing characteristics compared with both pristine PANI and PANI-AIL. Therefore, PANI-PIL emerges as a promising material for advanced supercapacitor electrodes and electrochemical sensing applications, showing the potential of ionic liquid doping as an effective approach for improving the performance of conducting polymers.

## Credit authorship contribution statement

Yahya A. Ismail: Conceptualization, Supervision, Resources, Writing: review & editing, Project administration, Methodology. Afeefa Saliha A M: Major investigation, Writing-original draft, Formal analysis, Sivakrishna Prakash : Methodology, Investigation, Writing: review & editing, Validation, Lijin Rajan: Writing: review & editing, Validation, Formal analysis.

## Acknowledgments

The Authors gratefully acknowledge the Central Sophisticated Instrumentation Facility (CSIF), University of Calicut, Kerala, India for providing analysis facilities and M. S. Thayyil for conductivity studies. A M Afeefa acknowledges University of Calicut for the financial support via Research Fellowship. L. Rajan acknowledges Kerala State Council for Science, Technology and Environment (KSCSTE), Kerala, India for their financial support via research fellowship. S. Prakash acknowledge UGC, India for providing their research fellowship.

## Author Information

### Authors and affiliations

*Advanced Materials Research Center, Department of Chemistry, University of Calicut, Thenjipalam, 673635, India.*

Afeefa Saliha A M , Sivakrishna Prakash, Lijin Rajan.

## Corresponding author

Correspondence to Yahya A Ismail

## Ethics declarations

## Conflicts of interests

The authors declare that they have no conflict of interest.

1. Shabeeba, A., et al., *Polypyrrole/hydrogel hybrid films as multi sensing supercapacitor electrodes.* Journal of Energy Storage, 2022. **55**: p. 105724.
2. Ajayan, A., et al., *Macromolecular sensing motors from conducting polymers: polyaniline/methylcellulose composites as stable current sensing supercapacitors.* International Journal of Biological Macromolecules, 2024. **279**: p. 135312.
3. Rawat, M., et al., *Characterization of Tuned Conducting Polymers*, in *Tuning of Conducting Polymers: Applications from Environmental to Biomedical Fields*. 2026, Springer. p. 43-61.
4. Kausar, A., *Overview on conducting polymer in energy storage and energy conversion system.* Journal of Macromolecular Science, Part A, 2017. **54**(9): p. 640-653.
5. Alburaih, H.A., et al., *Synergistic Effect of Conducting Polymer PANI on Electrochemical Performance of Ni Ferrites for Asymmetric Supercapacitors.* Journal of Inorganic and Organometallic Polymers and Materials, 2025. **35**(10): p. 8613-8626.
6. Bhawna, et al., *Boosting supercapacitor performance and thermal stability: transforming PANI nanorods into a ternary interconnected mesh structure.* Emergent Materials, 2025. **8**(5): p. 3707-3728.
7. Kianfar, E., *Conducting Polymer Nanocomposites for Electronics: Materials, Mechanisms, and Applications.* Journal of Inorganic and Organometallic Polymers and Materials, 2025: p. 1-54.
8. Zhu, S., Y. Huang, and B. Fang, *Progress and prospect for conducting polymer fibers.* Advanced Materials, 2025. **37**(48): p. e04071.
9. Le, T.-H., Y. Kim, and H. Yoon, *Electrical and electrochemical properties of conducting polymers.* Polymers, 2017. **9**(4): p. 150.
10. Namsheer, K. and C.S. Rout, *Conducting polymers: a comprehensive review on recent advances in synthesis, properties and applications.* RSC advances, 2021. **11**(10): p. 5659-5697.
11. Su, D., et al. *Conducting polymers in supercapacitor application*. in *IOP Conference Series: Earth and Environmental Science*. 2019. IOP Publishing.
12. Rajan, L., et al., *Conducting polymers as bio-mimetic multistep macromolecular sensors of working conditions: polyindole/polyvinyl alcohol hybrid film senses electrical and chemical working ambient.* Materials Chemistry Frontiers, 2022. **6**(12): p. 1706-1718.
13. Gharahcheshmeh, M.H. and K. Chowdhury, *Fabrication methods, pseudocapacitance characteristics, and integration of conjugated conducting polymers in electrochemical energy storage devices.* Energy Advances, 2024. **3**(11): p. 2668-2703.
14. Shahid, M.A., et al., *Advances in conductive polymer-based flexible electronics for multifunctional applications.* Journal of Composites Science, 2025. **9**(1): p. 42.

15. Masood, M., et al., *Recent progress, challenges, and opportunities of conducting polymers for energy storage applications.* ChemistrySelect, 2024. **9**(23): p. e202302876.
16. Prakash, S., et al., *Polyaniline-Functionalized Sulfur and Nitrogen Co-Doped rGO: Toward Sustainable, Ultra-Stable Supercapacitors with Superior Energy Density and High Retention Rate.* Materials Research Bulletin, 2025: p. 113966.
17. Zhang, X., et al., *PEDOT: PSS: From conductive polymers to sensors.* Nanotechnology and Precision Engineering, 2021. **4**(4).
18. Shamshina, J.L. and P. Berton, *Ionic liquids as designed, multi-functional plasticizers for biodegradable polymeric materials: a mini-review.* International Journal of Molecular Sciences, 2024. **25**(3): p. 1720.
19. Mohapatra, P. and A.K. Barick, *Ionic liquids based polymer electrolytes for supercapacitor applications.* Journal of Power Sources, 2025. **626**: p. 235749.
20. Mousa, N., B. Abu-Jdayil, and A.Y. Zekri, *Recent Advances in the Utilization of Imidazolium-Based Ionic Liquids for Chemical-Enhanced Oil Recovery: A Comprehensive Review.* The Chemical Record, 2025. **25**(12): p. e202500096.
21. Pereira, J., et al., *An overview of the ionic liquids and their hybrids operating in electrochemical cells and capacitors.* Ionics, 2024. **30**(8): p. 4343-4385.
22. Shamsuri, A.A., et al., *Polymer composites containing ionic liquids: a study of electrical conductivity.* Electronic Materials, 2024. **5**(4): p. 189-203.
23. Liu, R., et al., *Influence of polyaniline films with different oxidation states on molecular adsorption and photocatalytic performance in the visible-infrared light region.* Journal of Colloid and Interface Science, 2025: p. 139401.
24. Shen, L. and X. Huang, *Electrochemical polymerization of aniline in a protic ionic liquid with high proton activity.* Synthetic Metals, 2018. **245**: p. 18-23.
25. Trchová, M., et al., *FTIR spectroscopic and conductivity study of the thermal degradation of polyaniline films.* Polymer Degradation and Stability, 2004. **86**(1): p. 179-185.
26. Trchová, M., et al., *Conducting polymer and ionic liquid: Improved thermal stability of the material–A spectroscopic study.* Polymer degradation and stability, 2014. **109**: p. 27-32.
27. Lenin, R., A. Singh, and C. Bera, *Effect of dopants and morphology on the electrical properties of polyaniline for various applications.* Journal of Materials Science: Materials in Electronics, 2021. **32**: p. 24710-24725.
28. Sahana, B., et al., *Chemically polymerized polyaniline: a study on the role of dopants and surfactants in modifying multi-functional properties.* Colloid and Polymer Science, 2026: p. 1-21.
29. Rafiq, S., et al., *Structure controlled enhanced photocatalytic activity of polyaniline (PANI).* Heliyon, 2025. **11**(4).
30. Kumar, A., et al. *Synthesis and thermal analysis of polyaniline (PANI)*. in *Journal of physics: conference series*. 2020. IOP Publishing.
31. Blinova, N.V., et al., *Control of polyaniline conductivity and contact angles by partial protonation.* Polymer International, 2008. **57**(1): p. 66-69.
32. Jafarzadeh, S., et al., *Direct measurement of colloidal interactions between Polyaniline surfaces in a UV-curable coating formulation: the effect of surface Hydrophilicity/hydrophobicity and resin composition.* Langmuir, 2014. **30**(4): p. 1045-1054.
33. Cao, Z. and Y. Xia, *Synthesis and tribological properties of polyaniline functionalized by ionic liquids.* Journal of Materials Science, 2018. **53**(9): p. 7060-7071.
34. Hattab, Y. and N. Benharrats, *New Simulation Methodology in Critical Behavior of the Doping Concentration and Conductivity Measurement of Synthesized Polyaniline.* Journal of Macromolecular Science, Part B, 2025. **64**(2): p. 150-158.
35. Sidheekha, M.P., L. Rajan, and Y.A. Ismail, *Reaction driven biomimetic sensing characteristics of polyaniline/chitosan hybrid film: sensing chemical and electrical reaction conditions.* Materials Chemistry and Physics, 2022. **279**: p. 125769.

36. Sidheekha, M.P., et al., *Characterization of polyanilines synthesized at different pH for electrochemical sensing and supercapacitor applications.* Materials Today: Proceedings, 2022. **51**: p. 2286-2292.
37. Rajan, L., et al., *Structural electrochemistry of poly (3, 4-ethylenedioxythiophene) and its applicability as simultaneous sensor of environmental surroundings: self-sensing electrical, thermal, and chemical working conditions.* Journal of Materials Chemistry A, 2024. **12**(8): p. 4583-4600.
38. Arias Pardilla, J., et al., *Biomimetic Sensing–Actuators Based on Conducting Polymers*. 2012: NY Research Press.
39. Rajan, L., et al., *Reaction Induced Conformational Change in Polyindole: Polyindole/PVA Film as Biomimetic Sensors of Temperature and Electrical Energetic Conditions.* Chemistry–An Asian Journal, 2023. **18**(22): p. e202300742.
40. Rajan, L., et al., *Biomimetic multi-sensing behavior through co-operative actuation of electro-chemical macromolecular motors in conducting polymers: Results from PEDOT/PVA interpenetrated films.* Sensors International, 2026: p. 100373.
41. Prakash, S., et al., *Covalently bonded polyaniline-nitrogen doped rGO macromolecules for superior supercapacitors with enhanced energy density and long-term cyclic stability.* Journal of Power Sources, 2026. **665**: p. 239079.
42. Rajamany, R., S. Prakash, and Y.A. Ismail, *Synthesis and characterisation of polyaniline/polyvinyl alcohol composites as supercapacitor electrode materials.* Plastics, Rubber and Composites, 2022. **51**(5): p. 240-249.
43. Martins, J.C., et al., *Electrochemical behavior of polyaniline: A study by electrochemical impedance spectroscopy (EIS) in low-frequency.* Solid State Ionics, 2020. **346**: p. 115198.
44. Barsoukov, E., *Impedance spectroscopy theory, experiment, and applications*. 2005: Wiley Online Library.
45. Yousif, N.M. and M.R. Balboul, *Electrochemical performance of flexible supercapacitor electrodes based on EVA/PANI@ CNT nano-composite.* Russian Journal of Electrochemistry, 2024. **60**(12): p. 1133-1152.